AD-A047 565 PENNSYLVANIA STATE UNIV UNIVERSITY PARK APPLIED RESE--ETC F/G 13/10
PROPELLER-HUB INTERFERENCE EFFECTS USING AN APPROXIMATE LIFTING--ETC(U)
JUN 77 K LUDOLPH N00017-43-C-1418
UNCLASSIFIED TM-77-198 NL

1 OF 2
AD
A047 565

PROPELLOR-HUB INTERFERENCE EFFECTS USING AN APPROXIMATE LIFTING SURFACE THEORY

Karl Ludolph

Technical Memorandum
File No. TM 77-198
June 15, 1977
Contract No. N00017-73-C-1418

Copy No. 5

The Pennsylvania State University
Institute for Science and Engineering
APPLIED RESEARCH LABORATORY
Post Office Box 30
State College, PA 16801

NAVY DEPARTMENT

NAVAL SEA SYSTEMS COMMAND

UNCLASSIFIED

SECURITY CLASSIFICATION OF THIS PAGE (When Data Entered)

REPORT DOCUMENTATION PAGE

READ INSTRUCTIONS BEFORE COMPLETING FORM

1. REPORT NUMBER: TM-77-198	2. GOVT ACCESSION NO.
3. RECIPIENT'S CATALOG NUMBER	
4. TITLE (and Subtitle): PROPELLOR-HUB INTERFERENCE EFFECTS USING AN APPROXIMATE LIFTING SURFACE THEORY	5. TYPE OF REPORT & PERIOD COVERED: M.S. Thesis, November 1977
	6. PERFORMING ORG. REPORT NUMBER: TM 77-198
7. AUTHOR(s): Karl Ludolph	8. CONTRACT OR GRANT NUMBER(s): N0017-43-C-1418
9. PERFORMING ORGANIZATION NAME AND ADDRESS: The Pennsylvania State University, Applied Research Laboratory, P. O. Box 30, State College, PA 16801	10. PROGRAM ELEMENT, PROJECT, TASK AREA & WORK UNIT NUMBERS
11. CONTROLLING OFFICE NAME AND ADDRESS: Naval Sea Systems Command, Department of the Navy, Washington, D. C. 20362	12. REPORT DATE: June 15, 1977 (15 Jun 77)
	13. NUMBER OF PAGES: 102 pages & figures
14. MONITORING AGENCY NAME & ADDRESS (if different from Controlling Office)	15. SECURITY CLASS. (of this report): Unclassified, Unlimited
	15a. DECLASSIFICATION/DOWNGRADING SCHEDULE

16. DISTRIBUTION STATEMENT (of this Report)

Approved for public release, distribution unlimited, per NSSC (Naval Sea Systems Command), 7/7/77

(1) Technical memo.

17. DISTRIBUTION STATEMENT (of the abstract entered in Block 20, if different from Report)

18. SUPPLEMENTARY NOTES

391 007

19. KEY WORDS (Continue on reverse side if necessary and identify by block number)

Lifting surface
Interference
Propeller
Airfoils
Lift Coefficient
Flow

20. ABSTRACT (Continue on reverse side if necessary and identify by block number)

In order to provide for a more exact model of a marine propeller with a hub and yet avoid the complex computations necessary in an exact theory, an approximate lifting-surface theory was developed. The approximation fundamental to this development is that of Weissinger's, where an airfoil is replaced with a single bound vortex and its associated trailing vortex system at the 1/4 chord point, while the boundary conditions are satisfied only at the 3/4 chord point. The life coefficient obtained in this manner will approximate the results of thin airfoil and be exactly the same for the cases of circular arc and flat plate airfoils.

DD FORM 1 JAN 73 1473 EDITION OF 1 NOV 65 IS OBSOLETE

UNCLASSIFIED

SECURITY CLASSIFICATION OF THIS PAGE (When Data Entered)

20. ABSTRACT (Continued)

This theory was subsequently used to find the induced normal velocity on the surface of a propeller's hub. The hub was broken up into a series of frustrums and the average induced velocity was found on an arc of the frustrum between two successive blades. This velocity was assumed constant over the entire frustrum. The induced normal velocity at each section of the hub was then incorporated into the A. M. O. Smith, and J. Pierce solution of the potential flow around an arbitrary body. Once this source distribution was found for uniform onset flow around the body and hub, the distribution was used along with the approximate lifting-surface theory to find the ideal lift coefficient, ideal angle of attack, and the maximum camber of the propeller section.

Three computer programs were written to apply this theory to an actual propeller and hub. Furthermore, they consider four different circulation distributions that are solutions of a lifting-line design problem. The results of the approximate lifting-surface theory were compared to those of the lifting-line via a camber correction term. Through this term, it was also possible to compare this theory with the more exact theories, and the approximation proved to work well for an order of magnitude comparison. There seemed to be a problem near the hub and tip due to the strong trailing systems there. The hub was found to induce a larger lift coefficient near the tip. Up to mid-span, however, it was concluded that its effect should not be neglected. It was further recommended that more control points in the chord-wise direction be used in the approximate lifting-surface theory. More points should enable the program to come closer to the trends in the exact theory and still avoid the complex numerical integrations.

ACKNOWLEDGMENTS

The author wishes to express his gratitude to Dr. Joseph J. Eisenhuth, his advisor, for his valuable guidance in the development of this thesis.

He would also like to thank Dr. Robert E. Henderson for his comments on the final manuscript, and the staff of the Garfield Thomas Water Tunnel for their assistance.

This research was performed for the Applied Research Laboratory at The Pennsylvania State University under sponsorship of the Naval Sea Systems Command, Code 035.

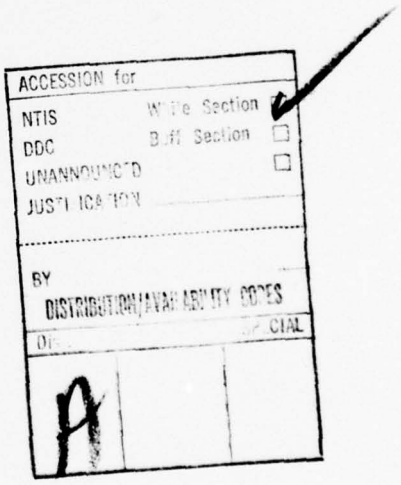

TABLE OF CONTENTS

LIST OF TABLES

LIST OF FIGURES

NOMENCLATURE

A_1	area denoted in Figure 1
A_2	area denoted in Figure 1
A_3	area denoted in Figure 1
$C(r)$	radial distribution of chord
C_T	thrust coefficient = $T/\frac{1}{2}\rho V_o^2 \pi R_B^2$
dr	length of bound vorticity
ds	length of free vorticity
$\frac{df}{dx}$	slope of camber line
$\frac{dz}{dx}$	slope of camber line
$\frac{d\Gamma}{dr}$	strength of free vortex
K_c	camber correction factor
$P(r)$	pitch distribution of blades
$\vec{R}$	vector from control point to vorticity
R	propeller radius
R_B	maximum body radius
r	body radius
r_H	radius of hub
r_P	radial location of control point
R_{pr}	projected value of R in x-y plane
U_n	velocity induced by entire vortex system
U	same as V_ℓ
V	axial velocity
V_o	free-stream velocity
V_B	velocity induced by bound system
V_{Ba}	axial component of V_B

V_{BL}	tangential component of V_B
$\vec{V}_{BH}$	bound velocity at hub
$\vec{V}_e$	velocity in propeller wake
$\vec{V}_{f_1}$	velocity induced by free system over A_1
$\vec{V}_{f_2}$	velocity induced by free system over A_2
$V_{f_{1a}}$	axial component of V_{f_1}
$\vec{V}_{f_{1t}}$	tangential component of V_{f_1}
$\vec{V}_{f_H}$	velocity induced by free system at hub
$\vec{V}_i$	velocity induced in Biot Savart Law
V_ℓ	velocity induced by free vortex system of the original lifting line
W_n	Un-U
w	velocity induced by lifting line
x	radial position normalized with respect to propeller radius; also distance along chord
Z	axial distance between 1/4 chord and point on hub
$Z_{1/4}$	axial position of 1/4 chord
Z_p	axial position of point on hub
α_i	ideal angle of attack
β	pitch angle
Γ_c	free circulation distribution
Γ_r	bound circulation
θ	angular coordinate
$\theta_{1/4,3/4}$	angular coordinate of 1/4, 3/4 chord point of control point
$\theta_{1/4',3/4}$	angular coordinate of 1/4, 3/4 chord point of vorticity

Chapter I

INTRODUCTION

1.1 General Statement of the Problem

Marine propellers are the primary means of propulsion through water. Operating in a liquid, however, presents a unique series of design problems that are not found in propellers that operate in air. The marine propeller blades must have a low aspect ratio and if the propeller is to operate on the aft portion of a body, it often requires a sizable hub, a fact that leads to theoretical complications.

In designing low aspect ratio blades, the "lifting-line" approach (i.e., the blade is replaced by a single bound line of vorticity) is not totally adequate as a theoretical model for design. It is necessary then to use a lifting-surface approach or provide some sort of correlation to the lifting-line model. Lifting-surface methods are not without problems for they are usually cumbersome and require many complex computations which lead to much time on a computer.

The hub's effects will be felt more prominently in the inboard areas of the blade and require changes in the camber when designing those blade sections. Although these effects must decrease rapidly in the radial direction, the effect of the hub must not be ignored in the design problem.

The effects just mentioned are accentuated and altered with the use of skewed propeller blades. Skew is defined as the displacement of the midchord points of the blade sections in the relative flow direction from their normal radial reference line location. Although methods presently exist for handling the two effects for straight blades, it is desirable

to develop an approach that can be extended to the skewed case without any extreme changes in the type of model used.

1.2 Previous Investigations

The theoretical problem of the propeller was first solved by Goldstein in Reference 1. He obtained the bound circulation of the blade through a semi-infinite series of modified Bessel functions of the first kind and Lommel's functions. The coefficients of the Bessel functions were determined by an infinite number of simultaneous equations. In this analysis and Prandtl's approximation to Goldstein's solution in Reference 2, the circulation distribution extends to the axis of rotation. A hub is not considered.

McCormick in Reference 3 solved the problem of the optimum propeller where the hub was approximated by an infinitely long circular cylinder concentric to the axis. The strengths in the trailing vortex sheet were adjusted so that the normal velocity on the surface of the cylinder was zero. The results obtained were ratios of circulation with a hub to circulation without a hub. Thus, all that was necessary was to multiply the Goldstein Kappa Factor or Prandtl's F-factors by this ratio and then proceed as in the no-hub case. Another solution along the same lines as those developed by McCormick but with different boundary conditions is reported in Reference 4 by Tachmindji.

Wald in Reference 5 restates the problem as that of finding the circulation distribution surrounding a finite hub which is transformed into true helicoidal sheets at the end of the hub. The solution is then carried through for the case of an infinitely-bladed propeller with an approximation for the case of a small number of blades.

All of the abovementioned endeavors use a lifting-line model of the propeller. A complete review of lifting surface theories will not be given here because there are more than adequate reviews given by Wu in Reference 6 and Isay in Reference 7. However, it would be useful to cover briefly the work of Pien in Reference 8 for the study being reported here follows similar lines.

The starting point of Pien's paper is the original lifting line of the blade. This lifting line is restored to a lifting surface by distributing the circulation $\Gamma(r)$ at each radius along the chord of the lifting surface where:

$$\Gamma(r) = \int_{\theta(r)_T}^{\theta(r)_L} \Gamma_r(r,\theta)d\theta \quad . \tag{1}$$

In the ultimate wake, there is a free circulation given by:

$$\Gamma_c(r) = -\frac{d\Gamma(r)}{dr}\,dr \quad . \tag{2}$$

Combining Equations (1) and (2) yields:

$$\Gamma_c(r) = -[\frac{d}{dr}\int_{\theta(r)_T}^{\theta(r)_L} \Gamma_r(r,\theta)d\theta]dr \quad , \tag{3}$$

which by the Leibniz formula results in

$$\Gamma_c(r) = -dr\int_{\theta(r)_T}^{\theta(r)_L} \frac{\partial\Gamma_r(r,\theta)}{\partial r}\,d\theta - \Gamma_r[r,(r)_L]\frac{d\theta(r)_L}{dr}\,dr + \Gamma_r[r,(r)_T]\frac{d\theta(r)_T}{dr}\,dr \quad . \tag{4}$$

The free or trailing circulation in the lifting surface $\Gamma_\theta(r,\theta)$ is thus:

$$\Gamma_\theta(r,\theta) = -\Gamma_r[r,\theta(r)_L)\frac{d\theta(r)_L}{dr}\,dr - dr\int_{\theta}^{\theta(r)_L}\frac{\partial\Gamma_r(r,\theta)}{\partial r}\,d\theta \qquad (5)$$

$$\theta(r)_L \geq \theta \geq \theta(r)_T \quad .$$

Pien next found the induced velocity at a point P due to these Γ-distributions. He found the velocity induced by the bound circulation system, by the free-vortex system within the blade itself, and finally by the free-vortex system extends to infinity. To completely avoid the integration over an infinite area, he superimposed a lifting line of circulation Γ(r) through the point in question as shown in Figure 1.

After a clever manipulation of the equation for the boundary conditions which will be shown later, the integral to infinity is eliminated. However, Pien was still left with some rather formidable double integrations which have to be evaluated numerically.

Nelson in Reference 9 suggests a method in which the hub boundary condition is included in lifting surface propeller design. He derives a procedure for using the Douglas program to model a hub. The body is approximated as a patchwork of four-sided plane elements, and a source strength is determined, such that there is no flow through the element. Nelson believes that the program can be altered for an arbitary normal velocity at each element caused by a propeller vortex system. Once the effect of the propeller is known, the hub can be used to find its effect on the propeller blade itself in terms of induced velocities.

1.3 Statement of Scope of Problem

This investigation is divided into two parts. The first part is concerned with the development of an approximate lifting-surface theory

to avoid at least part of the numerical integrations Pien derived. This approach will be limited to a nonviscous fluid and only the potential flow case is considered.

The second part is concerned with using this theory in conjunction with a potential flow model of a hub to examine how the hub affects the design process. By solving first for how the propeller system affects the hub, then using these data in modeling the hub, a new propeller design program is developed. This program uses an approximate lifting-surface theory and takes into account these hub effects. This second part is also limited to a nonviscous fluid and only the potential flow case is considered.

Chapter II

DEVELOPMENT OF A LIFTING-SURFACE THEORY USING THE WEISSINGER APPROXIMATION

2.1 Introduction

The point of lifting-surface theory is to have the bound vorticity distributed along the chord of the surface instead of concentrated along a line. Since the integration must then be performed over a surface rather than a line, the mathematics involved will be much more complex but the result should more accurately represent what is happening.

In this section, the development of a lifting-surface theory for marine propellers will be carried out along lines similar to that used by Pien in Reference 8. However, the resulting integrals will be simplified by the use of Weissinger's approximation. This approximation is used so that the complexity of the calculations will be reduced when trying to incorporate the calculation of hub effects and when trying ultimately to extend the approach to skewed propellers.

2.2 Boundary Condition Equations

Starting with the equation for circulation developed in Chapter I, the Biot-Savart law can be used to derive their associated induced velocities.

In its most general form, the Biot-Savart law reads:

$$d\vec{V}i = \frac{\gamma}{4\pi} \frac{\vec{r} \times d\vec{s}}{|\vec{r}|^3} \tag{6}$$

For a bound vortex element in Figure 2, the induced velocity becomes:

$$\vec{dV}_B = \frac{1}{4\pi} \frac{\Gamma_r(r,\theta)d\theta(\vec{R} \times \vec{dr})}{R^3}, \tag{7}$$

or in integral form:

$$\vec{V}_B = \frac{1}{4\pi} \iint_{A_1} \frac{\Gamma_r(r,\theta)d\theta(\vec{R} \times \vec{dr})}{R^3} \quad . \tag{8}$$

This area A_1 corresponds to that shown in Figure 1. For the free-vortex elements (see Figure 3), the induced velocities are:

$$\vec{V}_{f_1} = \frac{1}{4\pi} \iint_{A_1} \Gamma_\theta(r,\theta) \left(\frac{\vec{R} \times \vec{ds}}{R^3}\right) \quad , \tag{9}$$

$$\vec{V}_{f_2} = \frac{1}{4\pi} \iint_{A_2} - \frac{d\Gamma(r)}{dr} dr \frac{(\vec{R} \times \vec{ds})}{R^3} \tag{10}$$

and

$$\vec{V}_\ell = \frac{1}{4\pi} \iint_{A_3} - \frac{d\Gamma(r)}{dr} dr \frac{(\vec{R} \times \vec{ds})}{R^3}$$

$$+ \frac{1}{4\pi} \iint_{A_2} - \frac{d\Gamma(r)}{dr} dr \frac{(\vec{R} \times \vec{ds})}{R^3} \quad . \tag{11}$$

The area A_3 is located between the lifting line and the trailing edge of the blade.

From these velocity equations and the definition of areas of integration given in Figure 1, the appropriate boundary condition equation on the surface of the blade is developed. Figure 4 shows this boundary condition vectorially, and the equation that results from this figure is:

$$\frac{df}{dx} = \alpha_i - \left(\frac{U_n}{V_e} - \frac{U}{V_e}\right) \quad . \tag{12}$$

U_n is the velocity induced at any point along the camber by the entire vortex system previously described. The velocity term therefore represents the additional induced velocity due to the consideration of a lifting surface rather than a lifting line.

From the induced velocities derived earlier:

$$U_n - U = \vec{V}_B + \vec{V}_{f_1} + (\vec{V}_{f_2} - \vec{V}_\ell) \quad . \tag{13}$$

Substituting the integral expressions for these velocities yields:

$$U_n - U = \frac{1}{4\pi} \iint_{A_1} \Gamma_r(r,\theta) d\theta \frac{(\vec{R} \times d\vec{r})}{R^3} + \frac{1}{4\pi} \iint_{A_1} \Gamma r_\theta(r,\theta) \frac{\vec{R} \times d\vec{s}}{R^3}$$

$$+ \frac{1}{4\pi} \iint_{A_3} \frac{d\Gamma(r)}{dr} dr \frac{\vec{R} \times d\vec{s}}{R^3} \quad . \tag{14}$$

In no case is the integration performed to infinity. This is a great simplification, but nevertheless the work involved in evaluating the integrals is difficult. One of the difficulties arises as R goes to zero near vortex. In this case, the integral blows up. The difficulty will be avoided by resorting to the approximate lifting theory of Weissinger's. This theory states that if an airfoil is replaced with a single bound vortex at the 1/4 chord point and the boundary conditions are satisfied at the 3/4 chord point, the lift coefficient obtained will be the same as that obtained from thin airfoil theory. This approximation works exactly for circular arc and flat plate airfoils, and will be used here to develop the velocity expressions in a usable form.

2.3 The Bound Vortex System

From the last section, the velocity induced by the bound vortex system is:

$$V_B = \frac{1}{4\pi} \iint_{A_1} \frac{\Gamma_r(r,\theta)(\vec{R} \times d\vec{r})}{R^3} d\theta \quad . \tag{15}$$

$\vec{R}$ is the position vector directed from any point P to the location of a segment of the vortex line. Figure 2 shows the geometry of the situation where the view is upstream along the propeller axis and moving with the blade, r_p is the radius location of point P, so $\vec{R}$ is then just the vector from P to the element of length $d\vec{r}$. From Figure 2 and its geometry:

$$\vec{R} = \vec{i}(r \cos \rho - r_p) + \vec{j}(r \sin \rho) + \vec{k}\left[\frac{P(r)\phi}{2\pi}\right] \tag{16}$$

and

$$d\vec{r} = \vec{i} \cos \phi \, dr + \vec{j} \sin \phi \, dr \quad . \tag{17}$$

P(r) is just the pitch of the propeller, more specifically, the pitch of the vortex line. The pitch would correspond to a helical line oriented at the angle ϕ and is defined as the axial distance generated in moving along this line for one revolution. For a fraction of a revolution corresponding to the angle ϕ, the axial distance of advance is just:

$$\text{Axial distance} = \frac{r\phi}{2\pi r} = \frac{P(r)\phi}{2\pi} \quad .$$

The cross product $\vec{R} \times d\vec{r}$ becomes:

$$\vec{R} \times d\vec{r} = \begin{vmatrix} i & j & k \\ r \cos \phi - r_p & r \sin \phi & \frac{P(r)\phi}{2\pi} \\ \cos \phi \, dr & \sin \phi \, dr & 0 \end{vmatrix} \tag{18}$$

and

$$\vec{R} \times d\vec{r} = \left[-\vec{i}\frac{P(r)\phi \sin\phi}{2\pi} + \vec{j}\frac{P(r)\phi \cos\phi}{2\pi} - \vec{k}\, r_p \sin \phi\right] dr \quad . \tag{19}$$

Going back to Figure 2, the projected value of $\vec{R}$ in the x-y plane is:

$$R_{pr} = \sqrt{r^2 - 2r_p r \cos \phi + r_p^2} \quad . \tag{20}$$

The component in the z-direction is $\frac{P(r)\phi}{2\pi}$, so:

$$R = \sqrt{R_{pr}^2 + \left(\frac{P(r)\phi}{2\pi}\right)^2} \quad . \tag{21}$$

Finally:

$$R = \{r^2 - 2rr_p \cos\phi + r_p^2 + [\frac{P(r)\phi}{2\pi}]^2\}^{1/2} \quad . \tag{22}$$

By applying Weissinger's approximation to this integral, it in effect becomes a finite segment of bound vorticity located between some r_1 and r_2. The value of $\Gamma(r)$ for such a segment is $\Gamma(r_o)$ which is the value at r_o halfway between the two radii. This $\Gamma(r_o)$ is then just a constant in this integration and can be brought outside the integral.

$$V_B = \frac{\Gamma(r_o)}{4\pi} \int_{r_1}^{r_2} \frac{[-\vec{i}\,\frac{P(r)\phi \sin\phi}{2\pi} + \vec{j}\,\frac{P(r)\phi \cos\phi}{2\pi} - \vec{k}\, r_p \sin\phi]dr}{\{r^2 - 2r\, r_p\cos\phi + r_p^2 + [\frac{P(r)\phi}{2\pi}]^2\}^{3/2}} \quad . \tag{23}$$

$P(r)$ is also assumed constant over the interval of integration, so the axial component of velocity induced by the bound system becomes:

$$V_{B_a} = \frac{-\Gamma(r_o)}{4\pi} \sin\phi\, r_p \int_{r_1}^{r_2} \frac{dr}{[r^2 - 2rrp\cos\phi + r_p^2 + (\frac{P(r_o)\phi}{2\pi})^2]^{3/2}} \quad , \tag{24}$$

which upon integration becomes:

$$V_{B_a} = \frac{-r_p\Gamma(r_o)\sin\phi}{4\pi} \left[\frac{(r - r_p\cos\phi)}{\{r_p^2\sin^2\phi + [\frac{P(r_o)\rho}{2\pi}]^2\}R}\right]_{r_1}^{r_2} \quad . \tag{25}$$

Similarly, for the tangential component:

$$V_{Bt} = \frac{\rho\cos\phi\, P(r_o)\Gamma(r_o)}{8\pi^2} \left[\frac{(r - r_p\cos\phi)}{\{r_p^2\sin^2\phi + [\frac{P(r_o)\phi}{2\pi}]^2\}R}\right]_{r_1}^{r_2} \quad . \tag{26}$$

2.4 The Free Vortex System

In using Weissinger's approximation, the free vortex system are the trailing vortices that originate from the segments of bound vorticity at the 1/4 chord points.

Referring to Figure 3, the magnitude of $\vec{r}$ is a constant, and the positive direction of the vortex is going upstream as determined by the right-hand rule. From this figure:

$$\vec{ds} = -\vec{i}\, r \sin\phi + \vec{j}\, r \cos\phi + \vec{k}\frac{P(r)}{2\pi} \tag{27}$$

and

$$\vec{R} = \vec{i}(r\cos\phi - r_p) + \vec{j}\, r \sin\phi + k[\frac{P(r)\phi}{2\pi}] \quad . \tag{28}$$

The value of Γ in this case is actually $\Delta\Gamma$ and it is defined positive for increasing slope of the Γ versus r curve. From the Biot-Savart law, the expression for V_{f_1} is:

$$\vec{V}_{f_1} = \frac{\Delta\Gamma}{4\pi}\int_{3/4c}^{1/4c} \frac{\vec{R} \times \vec{ds}}{R^3} \tag{29}$$

Once again evaluating the cross-product:

$$\vec{R} \times \vec{ds} = \begin{vmatrix} \vec{i} & \vec{j} & \vec{k} \\ r\cos\phi - r_p & r\sin\phi & \frac{P(r)\phi}{2\pi} \\ -r\sin\phi\, d\phi & r\cos\phi\, d\phi & \frac{P(r)d\phi}{2\pi} \end{vmatrix} \tag{30}$$

$$= \vec{i}[\sin\phi - \phi\cos\phi]\frac{rP(r)}{2\pi}\, d\phi + \vec{j}[-r\phi\sin\phi - r\cos\phi +$$

$$+ r_p]\frac{P(r)}{2\pi}\, d\phi + \vec{k}[r^2 - r_p r\cos\phi]\, d\phi \quad . \tag{31}$$

Substituting this result into the expression for V_{f_1}:

$$V_{f_{1a}} = \frac{\Delta\Gamma}{4\pi} \int_{\theta_{3/4c}}^{\theta_{1/4c}} \frac{r(r - r_p \cos\phi)d\phi}{R^3} \tag{32}$$

and

$$V_{f_{1t}} = \frac{\Delta\Gamma}{4\pi} \int_{\theta_{3/4c}}^{\theta_{1/4c}} \frac{\frac{P(r)}{2\pi}[r_p - r(\cos\phi + \phi\sin\phi)]d\phi}{R^3} . \tag{33}$$

From before:

$$R = [r^2 - 2rr_p \cos\phi + r_p^2 + (\frac{P(r)\phi}{2\pi})^2]^{1/2} . \tag{34}$$

Although r is constant, this integral is of a form that is not in the regular tables. Therefore, the integral must be evaluated numerically, and there are no problems in doing this so long as the limits are interpreted correctly.

2.5 The Limits of Integration for the Free Vortex System

This section will deal with a closer look at the limits of integration and take into account Weissinger's approximation as it applies to the sum $V_{f_1} + (V_{f_2} - V_\ell)$. This sum as shown in Equation (12) and (13) is an essential part of the boundary condition.

Referring to Figure 5, the easiest way to visualize how the limits of integration are employed in the above sum is to go directly into some examples.

First consider a segment of bound vorticity at $\theta'_{1/4c}$ and its effect at the point in the figure. From the definition of V_{f_1} and through the application of Weissinger approximation, the limits on V_{f_1} are from $\theta'_{1/4c}$ to $\theta'_{3/4c}$. Similarly for V_{f_2}, the limits would be from $\theta'_{3/4c}$ to ∞. From

the definition of V_ℓ, its vortex line can be positioned such that it passes through the point P. The limits for trailing vortex from this line would then be from $\theta_{3/4c}$ (not primed) to ∞. Since all three vortices share the same strength $\Delta\Gamma$ (they are shed from the same radial distance), they can be summed according to the given velocity summation. From this equation it can be seen that the contribution from $\theta_{3/4c}$ to ∞ cancels, but left is the segment from $\theta_{3/4c}$ to $\theta'_{3/4c}$. Therefore, the total limits of integration are from $\theta_{3/4c}$ to $\theta'_{1/4c}$. Similarly, consider the point P' in the figure and a vortex line at $\theta_{1/4c}$:

(1) Integrate V_{f_1} from $\theta_{1/4c}$ to $\theta_{3/4c}$.

(2) Integrate V_{f_2} from $\theta_{3/4c}$ to ∞.

(3) Integrate V_ℓ to $\theta'_{3/4c}$ to ∞, this vortex line passes through P'.

Therefore, these limits become from $\theta'_{3/4c}$ to $\theta_{1/4c}$. Again, the strength of these vortices are identical because they arise from the same radial distance.

2.6 Adaptation of Lifting-Surface Theory to Computer Methods

In Figure 6, there is a plot of a circulation distribution versus radial position as it is derived by the lifting-line design program outline in Appendix A. This curve is broken up into strips of constant Γ, where the value of Γ used for the segment is just the mean value of the strip. The difference in adjacent strips is the trailing of $\Delta\Gamma$ value or:

$$\Gamma(r_{m,n}) = \Gamma\left[\frac{r_n + r_{n-1}}{2}\right] \tag{35}$$

and

$$\Delta\Gamma_{n,n-1} = \Gamma(r_{mn}) - \Gamma_{n-1} \quad , \tag{36}$$

where m denotes mean and is not an index. Substituting these expressions into Equations (25) and (26) for the case of a point P located at the 3/4 chord point at a radius r_{m_1} would yield:

$$V_{Bal} = \sum_n \frac{-r_{m_1}\Gamma(r_{mn})\sin\Delta\theta}{4\pi} \chi \left[\frac{r - r_{m_1}\cos\Delta\theta}{\{r_{m_1}^2\sin^2\Delta\theta + [\frac{P(r_{mn})\Delta\theta}{2\pi}]^2\}R} \right]. \tag{37}$$

$\Delta\theta$ here depends on what point P we are dealing with and what Γ_r is being used:

$$\Delta\theta = \frac{C(r_{m,n})\cos\phi(r_{m,n})}{4r_{m,n}} + \frac{C(r_{m,1})\cos\phi(r_{m_1})}{4r_{m,1}} \quad , \tag{38}$$

or normalized with respect to R_p:

$$\Delta\theta = \frac{\frac{C(r_{m,n})}{R_p}\cos\phi(r_{m,n})}{4X_{m,n}} + \frac{\frac{C(r_{m,1})}{R_p}\cos\phi(r_{m_1})}{4X_{m,1}} \quad . \tag{39}$$

From the earlier discussion on the limits of integration as they apply to the free vortex system, the integral expressions become:

$$V_{f_{a1}} + V_{f_{a2}} - V_{\ell_a} = \sum_n \frac{\Delta\Gamma_n}{4\pi} \int_{\theta_{3/4c(r_{m_1})}}^{\theta'_{1/4c(r_n)}} \chi$$

$$\left\{ \frac{r_n(r_n - r_{m_1}\cos\theta)d\theta}{[r_n^2 - 2r_n r_{m_1}\cos\theta + r_{m_1}^2 + (\frac{P(r_n)\theta}{2\pi})^2]^{3/2}} \right\} \tag{40}$$

and

$$V_{f_{t1}} + V_{f_{t2}} - V_{\ell_t} = \sum_n \frac{\Delta\Gamma}{\pi} \int_{\theta_{3/4c(r_{m_1})}}^{\theta'_{1/4c(r_n)}} \chi$$

$$\left\{ \frac{\frac{P(r_n)}{2\pi}[r_{m_1} - r_n(\cos\theta + \theta \sin\theta)]d\theta}{[r_n^2 - 2r_n r_{m_1}\cos\theta + r_{m_1}^2 + (\frac{P(r_n)}{2})^2]^{3/2}} \right\} . \qquad (41)$$

Once the equations for the velocities induced by the free and bound vortex distributions have been found, they can be used in conjunction with the hub to find the ideal lift coefficient and ideal angle of attack. This procedure is developed in Chapter V.

Chapter III

EXTENSION OF THE A.M.O. SMITH SOLUTION OF THE NEUMAN PROBLEM TO MODELING A HUB AND PROPELLER

3.1 Introduction

The A.M.O. Smith solution as given originally in Reference 10 and used by Pierce in Reference 11 was chosen to model the hub because of the simplicity of the program, its availability and the requirement for only an axisymmetric incoming flow. The body used in this endeavor is that of a typical underwater body shown in Figure 7. The effective hub region of the body is considered to extend about 3 body radii from the aft end of the body. This is the area where, based on calculated values, any significant mutual interference effects of propeller and hub will be felt.

3.2 Modeling the Hub

In the method developed by A.M.O. Smith for computing the potential flow about arbitrary axisymmetric bodies, the body is represented by series of rings or frustrums in the center of which is a ring source. The strength of each of these rings is determined by the condition that there is no fluid moving through the surface. Since the propeller will also induce some flow normal to the surface, it will be necessary to find exactly what this component of velocity is. This calculation will be performed in Chapter IV. Once this velocity is known for all the rings in the hub area, the source distribution is determined taking into account these normal velocities.

Naturally, in the area of the blades, a uniform flow can hardly exist. However, (referring to Figure 8) the average induced normal

velocity on the hub over the arc between two successive blades will be the same for any two other blades by symmetry arguments. This value of induced velocity will be used to find the new source distribution for the hub.

Chapter IV

ADAPTATION OF WEISSINGER'S LIFTING SURFACE THEORY TO FIND PROPELLER'S EFFECT ON THE HUB

4.1 Introduction

Before the hub can be successfully modeled using the A.M.O. Smith program, the induced velocities normal to the hub caused by the propeller vortex system must be calculated. The equations for these velocities will be developed analogously to the development of the approximate lifting surface theory in Chapter II. The A.M.O. Smith program, as seen previously, models the body by a distribution of ring sources. The strength of the source is assumed constant around the ring. This assumption is correct for an axisymmetric body in a uniform axisymmetric flow. However, the velocity induced by the propeller over the ring is not constant. An average velocity around the ring is then assumed. The hub is broken into segments of arc between two successive blades. This segment is further broken into ten elements and, once the velocity is found at each element, an average is obtained and spread around the hub over that particular frustrum.

4.2 The Bound Vortex System

The effect of the bound system will be considered first. From the Biot-Savart Law:

$$\vec{V}_B = \frac{1}{4\pi} \iint \frac{\Gamma_r(r,\theta)\, d\theta\, (\vec{R} \times d\vec{r})}{R^3} \quad . \tag{42}$$

Referring to Figure 9 which is an end view looking upstream,

$$\vec{R} = \vec{i}(r \cos\theta - r_H) + \vec{j}(r \sin\theta) + \vec{k}(Z_{1/4} - Z_p) \quad . \tag{43}$$

The component of $\vec{R}$ in the $\vec{k}$ direction is just the distance between the 1/4 chord point and the point in question as shown in Figure 9. In the case of a skewed blade outline, the 1/4 chord point of each blade section may not correspond to the same point on the body; therefore, the 1/4 chord position must be expressed as a function of radial position. Going back to Figure 9:

$$d\vec{r} = \vec{i} \cos\theta \, dr + \vec{j} \sin\theta \, dr \quad . \tag{44}$$

In order to take into account the effects of the other blades, θ is increased by 2π/number of blades. Solving the cross product:

$$\vec{R} \times d\vec{r} = \begin{vmatrix} i & j & k \\ r\cos\theta - r_H & r\sin\theta & Z_{1/4} - Z_P \\ \cos\theta \, dr & \sin\theta \, dr & 0 \end{vmatrix} \tag{45}$$

$$= [-\vec{i}(Z_{1/4} - Z_p)\sin\theta + \vec{j}(Z_{1/4} - Z_p \cos\theta) - \vec{k}(r_H \sin\theta)]dr \quad . \tag{46}$$

As before, the value of Γ used is the value at Γ_o which is halfway in between r_1 and r_2. Therefore,

$$\vec{V}_B = \frac{\Gamma(r)_o}{4\pi} \int_{r_1}^{r_2} \chi \; \frac{[-\vec{i}(Z_{1/4} - Z_p)\sin\theta + \vec{j}(Z_{1/4} - Z_p)\cos\theta - \vec{k}(r_H \sin\theta)]dr}{R^3} \quad . \tag{47}$$

Using the law of cosines and Figure 7, the projected values of $\vec{R}$ in the x-y plane becomes:

$$R_{pr} = r^2 - 2rr_H \cos\theta + r_H^2 \quad . \tag{48}$$

The total magnitude of $\vec{R}$ then becomes:

$$R = [r^2 - 2rr_H \cos\theta + r_H^2 + (Z_{1/4} - Z_p)^2]^{1/2} \quad . \tag{49}$$

The expression for the axial component of velocity can now be written:

$$V_{Ba_H} = \frac{-\Gamma(r_o R_H \sin\theta}{4\pi} \int_{r_2}^{r_2} \chi \frac{dr}{[r^2 - 2rr_H \cos\theta + r_H^2 + (Z_{1/4} - Z_p)^2]^{2/3}} \quad . \tag{50}$$

This can be integrated to yield:

$$V_{Ba_H} = \frac{-r_H \Gamma(r_o) \sin\theta}{4\pi} \left[\frac{(r - r_H \cos\theta)}{\{r_H^2 \sin^2\theta + (Z_{1/4} - Z_p)^2\}R} \right]_{r_1}^{r_2} \quad . \tag{51}$$

Likewise, for the radial component,

$$V_{Br_H} = \frac{-\Gamma(r_o)(Z_{1/4} - Z_p) \sin\theta}{4\pi} \left[\frac{(r - r_H \cos\theta)}{\{r_H^2 \sin^2\theta + (Z_{1/4} - Z_p)^2\}R} \right]_{r_1}^{r_2} \quad . \tag{52}$$

4.3 The Free Vortex System

Consider now the normal velocity induced at the hub by the free vortex system. From Figure 10 and the geometry involved, the elemental length of free vorticity is just:

$$\vec{ds} = -\vec{i}\, rd\theta \sin\theta + \vec{j}\, rd\theta \cos\theta + \vec{k}\frac{P(r)}{2\pi} d\theta \quad . \tag{53}$$

P(r), as before, is just the axial distance traveled by the propeller in one rotation. The vector $\vec{R}$ becomes:

$$\vec{R} = \vec{i}(r \cos\theta - r_H) + \vec{j}\, r \sin\theta + \vec{k}(Z_{1/4} - Z_p + \frac{P(r)\,\theta}{2\pi}) \quad . \tag{54}$$

In Figure 9, there is a closer look at the z component of the vector $\vec{R}$. The segment of free vorticity will be located somewhere between the 1/4 chord line and the 3/4 chord line. The axial distance from point P to such a segment is constant for all blades so that it is unnecessary to

increase this angle θ by 2π/number of blades. A better representation for the z component and the one used in the computer program is:

$$Z_{1/4} - Z_p + X_n \sin \theta \ , \tag{55}$$

where X_n is the distance from the 1/4 chord point on the blade to the segment of vorticity in question, and ϕ is the pitch angle of that blade section.

A similar correction must be made for the angle θ. This angle must be corrected for the displacement of the trailing vortex system as it moves downstream. This change in θ would be

$$\Delta\theta = \frac{C(x_n) \cos \theta}{2r_m} \ , \tag{56}$$

where r_m is the radial position of the vorticity. From Figure 10, this $\Delta\theta$ should be subtracted and the new value of θ is called θ'. Examining the cross product once again:

$$\vec{R} \times d\vec{s} = \begin{vmatrix} i & j & k \\ r \cos \theta' - r_H & r \sin \theta' & (Z_{1/4} - Z_p + X_n \sin \phi) \\ -r \sin \theta' \, d\theta & r \cos \theta' \, d\theta & \frac{P(r) \, d\theta}{2\pi} \end{vmatrix} \ . \tag{57}$$

and

$$\begin{aligned} \vec{R} \times d\vec{s} = {} & \vec{i}\left[\frac{r \sin \theta'}{2\pi} P(r) - r \cos \theta'(Z_{1/4} - Z_p + X_n \sin \phi)\right]d\theta \\ & -\vec{j}\left[(r \cos \theta' - r_H \frac{P(r)}{2\pi} + r \sin \theta'(Z_{1/4} - Z_p + X_n \sin \phi)\right]d\theta \\ & + \vec{k}[r^2 \cos^2 \theta' - r_H r \cos \theta' + r^2 \sin^2 \theta']d\theta \ . \end{aligned} \tag{58}$$

Let $Z = Z_{1/4} - Z_p$:

$$\vec{R} \times d\vec{s} = \vec{i}\left[\frac{\sin\theta' P(r)}{2\pi} - \cos\theta'(Z + X_n \sin\phi)\right]rd\theta$$

$$-\vec{j}\left[(r\cos\theta' - r_H \frac{P(r)}{2\pi} + r\sin\theta'(Z + X_n \sin\phi)\right]d\theta$$

$$-\vec{k}[r^2 - r_H r\cos\theta']d\theta \ . \qquad (59)$$

Substituting this expression into the Biot-Savart law and breaking the result into components yields:

$$V_{fa_H} = \frac{\Delta\Gamma}{4\pi} \int_{\theta 3/4c}^{\theta 1/4c} \frac{r(r - r_H \cos\theta')d\theta}{R^3} \qquad (60)$$

and

$$V_{fr_H} = \frac{\Delta\Gamma}{4\pi} \int_{\theta 3/4c}^{\theta 1/4c} \frac{\left[\frac{\sin\theta' P(r)}{2\pi} - \cos\theta'(Z + X_n \sin\phi)\right]rd\theta}{R^3} \ , \qquad (61)$$

where R now becomes:

$$\vec{R} = [r^2 - 2rr_H \cos\theta' + r_H^2 + (Z_{1/4} - Z_p + X_n \sin\phi)^2]^{1/2} \ . \qquad (62)$$

As in the case of the free vortex integral in Chapter II, this integral must also be integrated numerically. Since the same vortex system (that was used in Chapter II) must be used to find the effect on the hub, the same limits of integration also must hold.

4.4 Calculation of Normal Velocity at the Hub Surface

Now that the axial and radial components of velocity induced by the free-vortex system at points on the body are known, they can be used to find the normal velocity on the hub.

The velocity normal to the surface can be found by using these components of velocity and the geometry of the hub. The part of the radial component normal to the surface of the hub is found by multiplying this quantity by the cosine of the angle between the free stream and the

tangent to the surface at that point. The portion of the axial component normal to the surface is found similarly by using the sine of that angle. The total velocity normal to the surface is just the vector sum of both these parts. From the geometry in Figure 7, a plus radial component will be out of the hub. This agrees with the axial flow. For example, the axial induced flow is aft or in the minus z direction, the angle of the hub is negative. The sine of a negative angle is negative, so there is a positive normal flow out of the hub.

Chapter V

USING LIFTING SURFACE THEORY TO FIND BLADE SECTION CHARACTERISTICS

5.1 Introduction

In this chapter, the various induced velocities found in Chapter III will be combined with those induced by the hub. These velocities will be substituted back into the boundary condition equations. From that equation, the ideal lift coefficient, ideal angle of attack and camber line will be found.

5.2 Calculation of the Velocity Induced by the Hub

Once the source distribution around the body has been found, it is possible to find how this distribution induces a velocity at the control points on the blades. The body coordinates of each of the ring sources are used in conjunction with the coordinates of the control points on the blades. These coordinates are used to find the distance between the source and the point in question.

The induced velocity due to the individual ring sources is then summed over the body. Since the body is axisymmetric, there will be no tangential component of velocity. Furthermore, the radial component of induced velocity is of no concern to the design of the propeller blades. This component does not enter into the boundary condition equations of the blade section. The only component needed is the induced axial component. This velocity is added to the axial induced velocity of both the free and bound vortex systems. A sign change is necessary because the positive x-direction of the potential flow program corresponds to the negative z-direction in the lifting surface program.

5.3 Calculation of Ideal Angle of Attack

The ideal angle of attack will now be calculated by using the boundary condition equation given in Chapter II and restricting the analysis to the cases of symmetrical camber lines. From Equation (12) in Chapter II:

$$\alpha_i = \frac{df}{dx} + \left(\frac{U_n}{V_e} - \frac{U}{V_e}\right) \quad , \tag{63}$$

where $\frac{df}{dx}$ is the slope of the camber line of the blade section. For a symmetrical camber line, the slope of this line will be zero at the 1/2 chord. Therefore, once the induced velocities are known at the 1/2 chord position, it is an easy matter to solve for the ideal angle of attack:

$$\alpha_i = \left(\frac{U_n}{V_o} - \frac{U}{V_o}\right) \quad . \tag{64}$$

From Chapter II, U_n is the induced velocity due to the entire vortex system, and U is just the induced velocity of the lifting line calculated in the lifting line program.

5.4 Calculation of the Ideal Section Lift Coefficient

From Reference 12, Equation (4.25), the slope of a symmetrical mean line is proportional to the ideal lift coefficient via the relations

$$\frac{dy}{dx} = \frac{C_{\ell_i}}{4\pi}\left[\ell n\left(1 - \frac{x_1}{c}\right) - \ell n\frac{x_1}{c}\right] \quad . \tag{65}$$

This $\frac{dy}{dx}$ is just the $\frac{df}{dx}$ of the boundary condition equation. So once α_i is solved for via Equation (64), $\frac{df}{dx}$ is known so that C_{ℓ_i} can now be determined. Since the control point is at 3/4 chord, which corresponds to x_1 in Equation (65), C_{ℓ_i} becomes:

$$(C_{\ell_i})_{L.S.} = -11.4385\left(\frac{dy}{dx}\right)_{3/4c} \quad . \tag{66}$$

5.5 Calculation of the Maximum Camber

Equation (65) can be integrated to find the maximum camber of the section. By the assumption that the maximum camber occurs at mid-chord:

$$\frac{y}{c} = -\frac{C_{\ell_i}}{4\pi}\left[\left(1 - \frac{x}{c}\right)\ell n\left(1 - \frac{x}{c}\right) + \frac{x}{2}\ln\frac{x}{c}\right] \quad . \tag{67}$$

So upon substituting for C_{ℓ_i} and the mid-chord position, the maximum camber becomes

$$\frac{y_m}{c} = -0.6309\left(\frac{dy}{dx}\right)_{3/4c} \quad . \tag{68}$$

Chapter VI

RESULTS

6.1 Introduction

In each of the three preceding chapters, a FORTRAN computer program was developed to apply the given theory to a propeller on a typical underwater body. In this chapter, the results of the computer programs will be examined.

6.2 Results of the Lifting Line Program

As mentioned in Chapter II, the starting point of the approximate lifting surface theory is the original lifting line design problem. For the cases considered herein, the propeller has seven blades, a C_T of 0.1, the radius of the propeller is 8.00", the radius of the hub is 3.46" and the body radius is 10.5". The propeller is operating at an advance ratio of 2.0 and the velocity distribution in the wake is given in Table I. These data are used as input to the lifting line design program along

Table I

VELOCITY DISTRIBUTION IN WAKE OF THE BODY

x	V/V_o
0.4325	0.415
0.4594	0.465
0.5250	0.572
0.5906	0.659
0.6563	0.730
0.7219	0.788
0.7875	0.835
0.8531	0.8745
0.9188	0.9065
0.9844	0.9335
1.0500	0.954
1.1813	0.979
1.3135	0.990

with the maximum value of bound circulation as well as its radial position. It is possible to specify the value of circulation at the hub. Since the lifting line design method is well documented in Reference 13, it will not be discussed here; however, a listing of the FORTRAN program will be found in Appendix A.

There are three main outputs to the lifting line program. First the program specifies the circulation distribution necessary to give the specified C_T. It then gives the values of the ideal lift coefficient and induced velocities for all the stations. For the four cases dealt with here, the circulation distributions are shown in Figures 11-14.

6.3 The Propeller Interference Program

The circulation distribution shown in Figures 11-14 are then placed (with the propeller hub coordinates) into the FORTRAN program that finds the normal velocities on the hub. The effective hub region of the body is considered to extend about 3 body radii forward of the aft end of the body. Given in Table II are the z and r values of the effective hub stations as well as the four induced normal velocities caused by the different vortex systems. The velocities are normalized with respect to V_o. The explanation of this program as well as a definition of variables and a program listing are given in Appendix B.

6.4 The A.M.O. Smith Solution of the Neuman Problem

The various normal velocities given in the preceding section are then used by the computer program that models the underwater body. Also given to the computer are the coordinates of the frustrums that model the body. Table III shows the coordinates of the ring sources that lie at the

Table II

NORMAL VELOCITIES INDUCED AT HUB

		Case 1	Case 2	Case 3	Case 4
z_{hub}	r_{hub}	V Normal	V Normal	V Normal	V Normal
124.61612	9.31314	0.00030	0.00030	0.00029	0.00029
126.26312	9.11014	0.00034	0.00034	0.00033	0.00033
127.90953	8.90680	0.00040	0.00040	0.00039	0.00039
129.55664	8.67545	0.00047	0.00047	0.00046	0.00046
131.20370	8.44409	0.00057	0.00057	0.00056	0.00056
132.85086	8.17354	0.00068	0.00068	0.00066	0.00066
134.49799	7.90300	0.00083	0.00083	0.00081	0.00081
136.14500	7.61124	0.00101	0.00101	0.00099	0.00098
137.79216	7.31948	0.00126	0.00126	0.00124	0.00122
139.43927	7.00958	0.00158	0.00157	0.00155	0.00152
141.08532	6.69969	0.00205	0.00202	0.00200	0.00196
142.73349	6.37105	0.00266	0.00262	0.00260	0.00253
144.37987	6.04240	0.00357	0.00349	0.00347	0.00335
146.02687	5.70254	0.00488	0.00473	0.00472	0.00449
147.65096	5.36269	0.00677	0.00647	0.00648	0.00605
149.32120	5.01585	0.00973	0.00910	0.00918	0.00829
150.96820	4.66900	0.01399	0.01254	0.01282	0.01079
152.35847	4.37080	0.01802	0.01474	0.01569	0.01119
153.74861	4.07260	0.01785	0.00935	0.01360	0.00266
155.31381	3.75529	-0.00399	-0.02515	-0.00372	-0.02440
156.87904	3.43797	0.07882	0.20276	0.04626	0.12951
158.44424	3.12066	-0.00132	0.02800	0.00004	0.02762
160.01010	2.80336	-0.01155	-0.00187	-0.00874	0.00187
161.57530	2.48612	-0.00967	-0.00586	-0.00798	-0.00350
163.13638	2.16881	-0.00699	-0.00508	-0.00577	-0.00378
164.70573	1.85149				

Table III

OUTPUT OF POTENTIAL FLOW SOLUTION OF THE BODY

z	r	Sigma 1	Sigma 2	Sigma 3	Sigma 4
0.0	0.700	-0.1566 E 00	-0.1566 E 00	-0.1566 E 00	-0.1566 E 00
0.0	2.100	-0.1561 E 00	-0.1561 E 00	-0.1561 E 00	-0.1561 E 00
0.0	3.500	-0.1549 E 00	-0.1549 E 00	-0.1549 E 00	-0.1549 E 00
0.0	4.900	-0.1522 E 00	-0.1522 E 00	-0.1522 E 00	-0.1522 E 00
0.0	6.093	-0.1448 E 00	-0.1448 E 00	-0.1488 E 00	-0.1448 E 00
0.014	6.669	-0.1045 E 00	-0.1045 E 00	-0.1045 E 00	-0.1045 E 00
0.104	6.917	-0.7727 E-01	-0.7727 E-01	-0.7727 E-91	-0.7727 E-01
0.240	7.164	-0.5353 E-01	-0.5353 E-01	-0.5353 E-01	-0.5353 E-01
0.367	7.329	-0.5272 E-01	-0.5272 E-01	-0.5272 E-01	-0.5272 E-01
0.511	7.493	-0.5107 E-01	-0.5107 E-01	-0.5107 E-01	-0.5107 E-01
0.676	7.658	-0.4347 E-01	-0.4347 E-01	-0.4347 E-01	-0.4347 E-01
0.858	7.822	-0.4697 E-01	-0.4697 E-01	-0.4697 E-01	-0.4697 E-01
1.052	7.987	-0.4534 E-01	-0.4534 E-01	-0.4534 E-01	-0.4534 E-01
1.373	8.234	-0.4499 E-01	-0.4499 E-01	-0.4499 E-01	-0.4499 E-01
1.845	8.564	-0.4218 E-01	-0.4218 E-01	-0.4218 E-01	-0.4218 E-01
2.400	8.893	-0.3429 E-01	-0.3429 E-01	-0.3429 E-01	-0.3429 E-01
3.077	9.222	-0.2716 E-01	-0.2716 E-01	-0.2716 E-01	-0.2716 E-01
3.921	9.552	-0.2012 E-01	-0.2012 E-01	-0.2012 E-01	-0.2012 E-01
5.396	9.964	-0.1291 E-01	-0.1291 E-01	-0.1291 E-01	-0.1291 E-01
8.067	10.353	0.3630 E-02	0.3630 E-02	0.3630 E-02	0.3630 E-02
9.807	10.497	0.1020 E-01	0.1020 E-01	0.1020 E-01	0.1020 E-01
14.831	10.499	0.5406 E-02	0.5406 E-02	0.5406 E-02	0.5406 E-02
24.729	10.499	0.1176 E-02	0.1176 E-02	0.1176 E-02	0.1176 E-02
34.627	10.499	0.3789 E-03	0.3790 E-03	0.3789 E-03	0.3789 E-03
44.526	10.499	0.1590 E-03	0.1591 E-03	0.1589 E-03	0.1590 E-03
54.425	10.499	0.6688 E-04	0.6709 E-04	0.6681 E-04	0.6694 E-04
64.323	10.499	0.8944 E-05	0.9227 E-05	0.8853 E-05	0.9028 E-05
74.221	10.499	-0.4799 E-04	-0.4760 E-04	-0.4812 E-04	-0.4788 E-04
84.120	10.499	-0.1389 E-03	-0.1384 E-03	-0.1391 E-03	-0.1388 E-03
94.019	10.499	-0.3673 E-03	-0.3664 E-03	-0.3676 E-03	-0.3671 E-03
103.917	10.499	-0.1195 E-02	-0.1193 E-02	-0.1196 E-02	-0.1195 E-02
109.329	10.488	-0.1047 E-02	0.1049 E-02	0.1046 E-02	0.1047 E-02
110.616	10.460	0.4142 E-03	0.4162 E-03	0.4134 E-03	0.4146 E-03
112.262	10.404	0.3422 E-02	0.3424 E-02	0.3422 E-02	0.3423 E-02
113.909	10.318	0.5055 E-02	0.5057 E-02	0.5054 E-02	0.5055 E-02
115.556	10.201	0.7894 E-02	0.7895 E-02	0.7893 E-02	0.7894 E-02
117.204	10.065	0.7261 E-02	0.7263 E-02	0.7260 E-02	0.7261 E-02
118.851	9.917	0.9020 E-02	0.9022 E-02	0.9019 E-02	0.9020 E-02
120.498	9.757	0.8414 E-02	0.8416 E-02	0.8413 E-02	0.8414 E-02
122.145	9.586	0.9956 E-02	0.9958 E-02	0.9955 E-02	0.9956 E-02
123.792	9.404	0.9317 E-02	0.9319 E-02	0.9315 E-02	0.9316 E-02
125.439	9.211	0.1079 E-01	0.1080 E-01	0.1079 E-01	0.1079 E-01
127.086	9.008	0.1012 E-01	0.1012 E-01	0.1012 E-01	0.1012 E-01
128.733	8.791	0.1221 E-01	0.1221 E-01	0.1221 E-01	0.1221 E-01
130.380	8.559	0.1156 E-01	0.1156 E-01	0.1155 E-01	0.1156 E-01
132.027	8.308	0.1456 E-01	0.1456 E-01	0.1456 E-01	0.1456 E-01
133.674	8.038	0.1397 E-01	0.1397 E-01	0.1397 E-01	0.1397 E-01

Table III (cont'd)

z	r	Sigma 1	Sigma 2	Sigma 3	Sigma 4
135.321	7.757	0.1536 E-01	0.1536 E-01	0.1536 E-01	0.1536 E-01
136.968	7.465	0.1481 E-01	0.1482 E-01	0.1481 E-01	0.1481 E-01
138.615	7.164	0.1593 E-01	0.1593 E-01	0.1592 E-01	0.1593 E-01
140.262	6.854	0.1543 E-01	0.1543 E-01	0.1542 E-01	0.1543 E-01
141.909	6.535	0.1659 E-01	0.1660 E-01	0.1659 E-01	0.1659 E-01
143.556	6.206	0.1615 E-01	0.1616 E-01	0.1614 E-01	0.1615 E-01
145.203	5.872	0.1666 E-01	0.1668 E-01	0.1665 E-01	0.1666 E-01
146.838	5.532	0.1665 E-01	0.1668 E-01	0.1664 E-01	0.1666 E-01
148.485	5.189	0.1598 E-01	0.1603 E-01	0.1598 E-01	0.1601 E-01
150.144	4.842	0.1584 E-01	0.1595 E-01	0.1585 E-01	0.1594 E-01
151.663	4.519	0.1572 E-01	0.1597 E-01	0.1578 E-01	0.1602 E-01
153.053	4.221	0.1522 E-01	0.1578 E-01	0.1539 E-01	0.1599 E-01
154.531	3.913	0.1375 E-01	0.1526 E-01	0.1413 E-01	0.1575 E-01
156.096	3.596	0.1718 E-01	0.2131 E-01	0.1673 E-01	0.2031 E-01
157.661	3.279	0.5309 E-02	-0.1070 E-01	0.9513 E-02	-0.1264 E-02
159.227	2.962	0.1652 E-01	0.1438 E-01	0.1592 E-01	0.1347 E-01
160.792	2.644	0.1726 E-01	0.1720 E-01	0.1673 E-01	0.1637 E-01
162.355	2.327	0.1690 E-01	0.1713 E-01	0.1664 E-01	0.1665 E-01
163.920	2.010	0.1732 E-01	0.1753 E-01	0.1720 E-01	0.1730 E-01

mid-points of the frustrums as well as their computed individual source strengths designated by the sigmas. This program is given in Appendix C.

6.5 Results of the Lifting-Surface Design Program

The source distribution given in the preceding table was used in the lifting-surface propeller design program given in Appendix D. This design program was run for each of the four cases under consideration. Furthermore, to enable a better visualization of the effect of the hub on the blade section characteristics the exact same design program was run without the hub source distribution.

In Figure 15-18, the various ideal lift coefficients are plotted versus their blade section. These lift coefficients include the results of the lifting line program and the lifting surface results with and without a hub. Perhaps the most striking feature of the plots, is how greatly the hub does affect the C_{ℓ_i}. This effect is more pronounced in Cases 2 and 4 where the value of bound circulation at the hub is zero. Nevertheless, in Cases 1 and 3 where the value of circulation at the hub is not zero, the hub effect is still important. By comparing Cases 1 and 3, one can see that the radial point of maximum circulation plays a role in the magnitude of the hub effect. By moving the point of maximum Γ out several inches, the entire hub effect is reduced. This same trend is also shown clearly in Cases 2 and 4.

An important results that can be seen from these figures, is the apparent lack of correspondence between the results of the lifting line theory and that of the lifting-surface theory. This disagreement is more pronounced in Cases 2 and 4 where the values of circulation at the hub are

zero. The fact that the bound vorticity near the hub is small, seems to imply that the free-vortex system causes the noncomformity.

In Table IV, the effects of the free-vortex system are examined for Case 1. Presented are the values of axial induced velocities due to the free-vortex system at those stations where the greatest jumps in C_{ℓ_i} occur as denoted in Figure 15. It will now be shown how these jumps occur, and if they are indeed accurate. From Figure 19, one can see, looking upstream at the trailing edge of the blade, the proper direction of circulation of the free vortex system. Now referring to Table IV, the effect of the free vorticity at Station 2 on Station 18 is small and in the negative axial direction. According to the theory developed in Chapter II, this corresponds to the downstream direction. This result agrees with Figure 19. As one moves out radially, considering the segments of free vorticity closest to the tip and Station 18, the magnitude of induced velocity increases as expected. At Station 9, however, the sign of the velocity changes. After looking at Figure 11, it is seen that this change in sign is due to passing the maximum point of the circulation distribution. From Figure 19, again the sign and direction of induced velocity agree. The magnitude of induced velocity continues to increase because of the decreased distance to Station 18. Once Station 18 is reached, the segments of free vorticity on either side of the point are in opposition so the net value of induced velocity is small. As is expected, the sign changes once again and the magnitude starts to decrease. The effect of these velocities on Station 19 is shown in the next column of Table IV. As is readily evident, the magnitudes and signs of the various velocities follow the same correct pattern. Out towards the tip, however, it is seen that there are less negative contributions. The lack

TABLE IV

AXIAL INDUCED VELOCITIES AT THE 3/4 CHORD CONTROL POINT DUE TO THE FREE VORTEX SYSTEM FOR CASE 1

Station of Vortex	Control Pt. 18	Control Pt. 19	Control Pt. 4	Control Pt. 5
2	-0.0006	-0.0005	-0.0181	-0.0104
3	-0.0019	-0.0017	-0.1193	-0.0425
4	-0.0030	-0.0026	+0.0214	-0.1557
5	-0.0039	-0.0034	+0.1832	+0.0100
6	-0.0042	-0.0036	+0.0703	+0.1704
7	-0.0036	-0.0034	+0.0039	+0.0519
8	-0.0016	-0.0014	+0.0102	+0.0138
9	+0.0010	+0.0009	+0.0034	-0.0042
10	+0.0035	+0.0029	-0.0086	-0.0102
11	+0.0069	+0.0057	-0.0118	-0.0135
12	+0.0018	+0.0094	-0.0137	-0.0154
13	+0.0186	+0.0144	-0.0148	-0.0163
14	+0.0289	+0.0216	-0.0152	-0.0166
15	+0.0464	+0.0329	-0.0153	-0.0164
16	+0.0820	+0.0499	-0.0149	-0.0158
17	+0.2199	+0.0833	-0.0137	-0.0146
18	-0.0082	+0.2224	-0.0129	-0.0135
19	-0.2394	-0.0086	-0.0120	-0.0125
20	-0.0978	-0.2418	-0.0113	-0.0117
21	-0.0633	-0.0989	-0.0106	-0.0109
TOTAL	-0.0086	+0.0772	-0.02325	-0.13379

of negative contributions causes an abrupt change in magnitude between the two stations. This change in the total velocity induced by the free vortex system between these two stations causes the abrupt change in ideal lift coefficient shown in Figure 11. This same abrupt change is shown in the last two columns of Table IV for two stations near the hub. It should be noted once again these effects are the results of the consideration of the free-vortex system and have nothing to do with the hub.

6.6 Camber Correction Factors

In order to compare the results of the approximate lifting surface theory developed herein to that of the more exact theories given in Reference 8 and 14, it became necessary to find a basis of comparison.

In both References 8 and 14, a camber correction factor is developed that is defined as the ratio of the lifting surface camber to the lifting line camber. The camber correction factors that came from the approximate lifting surface theory are shown in Tables V and VI. Those of Reference 14 for a 6-bladed propeller at the same ratio of advance appear in Table VII. The only two cases that provide a good basis for comparison are Cases 2 and 4 in Table V since they use a similar circulation distribution, and the hub is not considered. Since in the four cases developed here, the blade is of a simple rectangular shape with seven blades and both references have different blades shapes and numbers, a direct comparison is impossible. Suffice it to say that all the efforts show a large increase in the camber correction factor near the hub and tip and at the mid sections of the blades, the approximate results are near Reference 14's results. What differs greatly in this comparison is not the numbers

Table V

CAMBER CORRECTION FACTORS WITHOUT THE HUB

Station	Case 1	Case 2	Case 3	Case 4
2	0.120	40.400	0.040	94.400
3	0.139	5.020	0.124	16.200
4	0.169	0.373	0.188	4.471
5	0.359	0.727	0.297	1.060
6	0.466	1.357	0.324	0.289
7	0.561	1.593	0.543	1.045
8	0.640	1.742	0.752	1.464
9	0.700	1.854	0.937	1.700
10	0.737	1.919	1.084	1.830
11	0.741	1.901	1.183	1.920
12	0.716	1.836	1.241	1.967
13	0.648	1.707	1.247	1.959
14	0.539	1.523	1.192	1.900
15	0.370	1.265	1.052	1.748
16	0.114	0.896	0.798	1.511
17	0.232	0.357	0.402	1.136
18	0.176	0.419	0.260	0.542
19	1.868	1.720	1.146	0.350
20	3.810	4.760	4.285	2.667
21	12.600	18.500	16.777	12.182

Table VI

CAMBER CORRECTION FACTORS WITH THE HUB

Station	Case 1	Case 2	Case 3	Case 4
2	1.910	66.400	1.301	121.200
3	0.971	8.220	0.895	18.400
4	0.351	1.250	0.513	5.470
5	0.156	0.316	0.148	1.480
6	0.474	1.157	0.081	0.124
7	0.711	1.467	0.377	0.922
8	0.875	1.650	0.626	1.377
9	0.991	1.779	0.842	1.634
10	1.048	1.852	1.000	1.780
11	1.052	1.844	1.118	1.877
12	1.004	1.785	1.179	1.925
13	0.906	1.655	1.192	1.919
14	0.731	1.470	1.139	1.861
15	0.469	1.211	1.000	1.711
16	0.075	0.830	0.746	1.474
17	0.486	0.298	0.337	1.090
18	0.272	0.532	0.347	0.493
19	3.184	1.930	1.562	0.245
20	6.818	4.960	4.430	2.787
21	24.000	18.750	17.220	12.454

Table VII

MORGAN'S CAMBER CORRECTION FACTORS
N=6 λ=2.0

r	K_c
0.3	2.276
0.4	1.783
0.5	1.698
0.6	1.681
0.7	1.754
0.8	1.926
0.9	2.448

themselves, but the trend as one moves out radially. The jumps shown in the previous section do not appear in "exact" camber correction factors as they do in Table V. This leads one to believe that the blade outline is a critical parameter of the approximate lifting surface theory, and may cause the jumps in C_{ℓ_i}.

Chapter VII

SUMMARY AND CONCLUSIONS

7.1 Statement of the Problem

In the field of marine propeller design, it is highly desirable to have as accurate a theoretical model as is possible. In many cases, this model consisted of a propeller modeled by a lifting line or a lifting surface. In these works, the hub of the propeller often is assumed to be small, or that it had a negligible effect on the design process. In this study, an approximate lifting surface theory was developed around Weissinger's approximation, and this theory was used to find what the effect of the hub on the blades was and, if in fact, it could be neglected in the design process. Once the hub effect can be accurately predicted, this information can be used to obtain better marine propeller designs.

7.2 Procedure of the Investigation

The starting point of this effort was the development of an approximate lifting surface model using Weissinger's approximation. This theory was then used in a computer program that calculated the induced velocities caused by the propeller vortex system normal to the surface of the hub. To find these values of velocity, the hub was broken up into rings or frustrums. The normal velocity was calculated at 10 points over an arc of the frustrum between two successive blades. The average of these 10 velocities was assumed constant over the arcs between any other two successive blades and spread around the entire ring. Once these values of normal velocities were found, they were incorporated into the boundary condition of the A.M.O. Smith, J. Pierce solution of the potential flow

around arbitrary bodies. The output of this program was a source distribution that modeled an underwater body and the effect of its propeller. This source-sink distribution was then used to find the induced velocities caused by the hub at the control points on the propeller blades as part of the design program. The design program with the hub was compared with the same design program not using the hub. From this comparison, conclusions were drawn concerning the effect of the hub. The approximate lifting surface theory without the hub effect was then compared to the more exact theories using a camber correction term as the basis of comparison.

7.3 Results

The results of the approximate lifting surface design program clearly show that the hub has an effect on the blade section characteristics. The effect depended upon the hub contour, the type of circulation distribution, specifically the point of maximum circulation and whether or not the circulation at the hub was a finite value or zero.

By use of a camber correction term, a comparison was attempted between the approximate lifting-surface theory and a more exact theory shown by Morgan in Reference 14. Since the specific case considered here did not correspond exactly to Morgan's case in the number of blades or blade outline, an order of magnitude comparison had to be made. The values obtained herein came within 10% of Morgan's results in most cases. This result seems to justify the use of the approximate theory. Furthermore, the approximate theory correctly predicted the large increase of the factor at the hub and tip as shown in both Morgan's and Pien's

results. However, the approximate theory deviated somewhat from the exact theories of Pien and Morgan in between those points.

7.4 Conclusions

From the results shown, it is evident that at least for hub radii greater than 0.4R, it is necessary to consider the effect of a hub in the design of a propeller. It was also shown that the shape of the bound circulation is a factor in determining how great the hub effect will be. A smaller hub effect occurs as the maximum point of circulation on the blade is moved radially outward.

The use of the approximate lifting-surface theory seems to be justified because of the general agreement with the more exact theories of Pien and Morgan. The lack of the correlation with the more exact lifting-surface theories was due in part to the different blade profiles used as well as the different blade characteristics. The use of only one control point in the chordwise direction, however, had to hurt the overall model. Use of more control points by dividing the blade section into a series of flat plates would prove beneficial, and the increase in computation time and cost would be offset by the increase in accuracy of the propeller model.

The wild effects shown on the inboard portions of the blade are above and beyond the hub effect and these effects may even overshadow the hub effect in some cases.

The assumptions made in examining the velocities normal to the hub due to the propeller vortex systems show themselves to be fair. No glaring inconsistencies were seen in the results of this program; thus, the use of more vigorous modeling techniques of the hub, though they consider

nonaxisymmetric inflow, are not justified. The increase in accuracy obtained would not justify the increased cost.

7.5 Suggestions for Further Research

The computer program herein should be used to find at what size hub its effects can be ignored. Furthermore, different cases should be considered to make a direct comparison of this approximate lifting surface with the results of Reference 14. The propeller design program should be refined to use more control locations along the chord by breaking the blade up into a string of flat plates, each with its own 3/4 chord location, and the capability of considering propeller skew should be added as well as extension to the case of a counterrotating propeller.

REFERENCES

1. Goldstein, S., "On the Vortex Theory of Screw Propellers," Proceedings of the Royal Society, London England, Series A, Vol. 63, 1929, pp. 440-465.

2. Prandtl, L., Betz, A., "Vier Abhand Lungen zur Hydrodynamik und Aerodynamic," GöHengen, 1927.

3. McCormick, B., "The Effect of a Finite Hub on the Optimum Propeller," J. Aero. Sci., 22, No. 9, September 1955.

4. Tachmindji, A. J., "The Potential Problem of the Optimum Propeller with Finite Hub," International Shipbuilding Progress, Vol. 3, 27, November 1956, pp. 563-572.

5. Wald, Q., "The Distribution of Circulation on Propellers with Finite Hubs," ASME Paper 64-WA/UNT-4, November 1964.

6. Wu, T., "Some Recent Developments in Propeller Theory," Schiffstechnik, Vol. 12, No. 60, 1965.

7. Isay, W., Propeller Theorie Hydrodynamische Problems, Springer Verlag Publishers, 1964.

8. Pien, P., "The Calculation of Marine Propellers Based on Lifting Surface Theory," J. Ship Res., Vol. 5, No. 2, 1961.

9. Nelson, D., "Note on the Inclusion of the Hub Boundary Condition in Lifting Surface Propeller Design, unpublished note.

10. Smith, A. M. O. and Pierce, J., "Exact Solution of the Newman Problem Calculation of Noncirculatory Plane and Axially Symmetric Flows About or Within Arbitrary Boundaries," Douglas Aircraft Co., Report No. E326988, 1958.

11. Pierce, T., "Tunnel Wall Interference Effects on the Drag and Pitching Moment of an Axisymmetric Body," Ph.D. Thesis, The Pennsylvania State University, 1964.

12. Abbott, I. and Von Doenhoff, A., Theory of Wing Sections, Dover Publications, New York, 1959.

13. McCormick, B., Eisenhuth, J., and Lynn, J., "A Study of Torpedo Propellers, Part I, The Pennsylvania State University, Report NOrd 16597-5, 1956.

14. Morgan, W. and Slovic, V., "Propeller Lifting Surface Corrections," Society of Naval Architects and Marine Engineers, New York, New York, 1968.

Appendix A

LIFTING LINE DESIGN PROGRAM

Definition of FORTRAN Terms

ATA	efficiency
CLI	ideal lift
CLIF	design lift coefficient
CONJ	λ
CORP	normalized
CTP	propeller thrust coefficient
CP	power coefficient
FUNCTION F	Prandtl tip low factor
GOGM	gamma over gamma max
GOGH	normalized gamma value at hub
GOGMT	true gamma max
CRI	gamma value at the station in question
IPRNT	print flag
J	advance ratio
NB	number of blades
NDEL	number of stations on blade
NV	number of velocity points in wake
NCASE	number of cases
RR	actual distance from centerline
RH	hub radius
RP	propeller radius
V	velocity values in wake
WA	axial induced velocity

WT	tangential induced velocity
XO	normalized starting point of loop
XR	normalized position from centerline
XZ	new x coordinate taking into account streamline contraction
YR	station along blade

FORTRAN PROGRAM LISTING

```
      SUBROUTINE THRUS (CONJ,NB,GOVO,XX,VV)
      REAL NB
      COMMON SINTT,CAK,F,WT,WA,PHI,VE
      DATA PI/3.1415927/
      SINT=CONJ/(SQRT(1.0+CONJ**2))
      CAK=EXP((-NB*(1.0-XX)/(2.0*SINTT)))
      F=2.0/PI*ATAN(SQRT(1.0-CAK*CAK)/CAK)
      WT=NB*GOVO/(4.0*PI*XX*F)
      WA=-.5*VV+SQRT(VV*VV+4.0*(XX/CONJ-WT) *WT)*.50
      PHI=ATAN(VV+WA)/(XX/CONJ-WT))
      VE=SQRT((XX/CONJ-WT)**2+(VV+WA)**2)
      RETURN
      END
      SUBROUTINE CDFUN (CLI,TOCF,CDF)
      REAL LIFT (11)
      DIMENSION TOC(11),CDTOC(122)  ,SC(11),EL(11),A(11),B(11),C(11)
      DIMENSION CLIF(11),CD1(22),CD2(22),CD3(22),CD4(22),CD5(11)
      EQUIVALENCE (CDTOC(23),CDL(1)),(CDTOC(45),CD2(1)),(CDTOC(67),CD3(1)),
     -  (CDTOC(89),CD4(1)),(CDTOC(111),CD5(1))
      DATA LIFT/0.0,0.1,0.2,0.3,0.4,0.5,0.6,0.7,0.8,0.9,1.0/
      DATA TOC/5.0,6.0,7.0,8.0,9.0,10.0,11.0,12.0,13,0,14.0,15.0/
      DATA CDTOC/.00395,.00411,.00437.,00466,.00500,.00538,.00577,.00617,
     -  .00656,.00697,.00741,.00401,.00420,.00447,.00478,.00512,.00550,
     -  .00590,.00630,.00670,.00712,.00755/
      DATA CD1/.00424,.00442,.00470,.00502,.00538,.00577,.00618,.00660,
     -  .00702,.00745,.00791,.00458,.00473,.00500,.00533,.00570,.00612,
     -  .00655,.00700,.00745,.00791,.00839/
      DATA CD2/.00495,.00512,.00538,.00572,.00611,.00656,.00702,.00749,
     -  .00795,.00841,.00888,.00540,.00554,.00581,.00615,.00658,.00705,
     -  .00754,.00803,.00852,.00901,.00951/
      DATA CD3/.00591,.00608,.00636,.00674,.00719,.00768,.00818,.00868,
     -  .00919,.00971,.01024,.00638,.00662,.00698,.00738,.00785,.00837,
     -  .00890,.00943,.00996,.01049,.01104/
      DATA CD4/.00700,.00726,.00763,.00808,.00858,.00913,.00968,.01023,
     -  .01079,.01135,.01194,.00766,.00792,.00831,.00878,.00933,.00990,
     -  .01048,.01107,.01165,.01223,.01284/
      DATA CD5/.00833,.00863,.00904,.00953,.01008,.01069,.01131,.01193,
     -  .01254,.01315,.01378/
      DO 1 I=1,11
      J=1+(I-1)*11
      CALL SPFIT (11,TOC,CDTOC(J)  ,SC,EL,A,B,C)
      CALL SPGET (11,TOC,CDTOC(J)  ,SV,EL,TOCF,CLIF(I),CP,CDP)
    1 CONTINUE
      CALL SPFIT (11,LIFT,CLIF,SC,EL,A,B,C)
      CALL SPGET (11,LIFT,CLIF,SC,EL,CLI,CDF,CP,CDP)
      RETURN
      END
      SUBROUTINE GAMMG (N,A1,XMAX,XX,AM,SL,EL)
      DIMENSION XX(6),AM(6),SL(6),EL(6)
```

```
      XDIST=1.0-(XMAX+.10)
      DELX=XDIST/4.0
      XX(1)=0.0
      AM(1)=A1
      SL(1)=0.0
      XX(2)=XMAX
      AM(2)=1.0
      SL(2)=0.0
      BEGSL=0.0
      FINSL=1.1/XDIST
      XD=0.0
      N=5
      J=N-1
      DO 1 I=3,4
      XD=XD+DELX
      AM(J)=XD*FINSL
      XX(J)=1.0-XD
      SL(J)=-FINSL
      J=J-1
    1 CONTINUE
      XX(5)=1.0
      AM(5)=0.0
      SL(5)=-FINSL
      RETURN
      END
      FUNCTION F(J,NB,X)
      REAL J,NB
      DATA PI/3.141593/
      CONJ=J/PI
      SINTT=CONJ/(SQRT(1.0+CONJ**2))
      CAK=EXP (-NB *(1.0-X)/(2.0*SINTT))
      F=2.0/PI*ATAN(SQRT(1.0-CAK*CAK)/CAK)
      RETURN
      END
      REAL J(20),N (20)
      DIMENSION X(15),V(15),YR(50),GR(50),VSC(50),ELV(50),A(50)
      DIMENSION B(50),C(50),XR(50),VC(50),X2(50),RP(20)
      DIMENSION YM(50),XM(50),GRM(50)
      DIMENSION TITLE(20),XX(10),YY(10),SG(10),ELG(10)
      COMMON SINTT,CAK,F,WT,WA,PHI,VE
      DATA PI/3.1415927/
  100 FORMAT (215)
  101 FORMAT (2F10.5)
  102 FORMAT (20A4)
  103 FORMAT ('1',20A4)
  104 FORMAT ('0','VELOCITY DISTRIBUTION',/(' X='F10.5,5X,'VEL='F10.5))
  105 FORMAT ('OGENERAL INPUTS')
  106 FORMAT ('0','RT='F8.3,9X,'Y-PEAK='F8.3)
  107 FORMAT ('0'.'FIRST INTEGRATED VALUE, CT='F10.5,5X,'G/VORP='F10.5)
  108 FORMAT (8F10.5)
  109 FORMAT (3F10.5)
  110 FORMAT ('0','FOR ADDED DRAG TERM, CT='F10.5,5X,'G/VORP='F10.5)
  112 FORMAT ('0','CP='F15.5,5X,'EFF.='F15.5)
```

```
115 FORMAT ('0','RH='F8.3,9X,'G RATIO HUB='F8.3)
116 FORMAT ('0','CT='F8.4,8X,'(G/VO*RP)MAX='F8.3)
117 FORMAT ('0'),'C/RP='F10.5)
118 FORMAT ('0','CASE('I2,') INPUTS'/' NUMBER OF BLADES='F5.1,5X,
   -  'J='F7.2,5X,'RP='F7.3)
119 FORMAT ('0','    Y',9X,'X',8X,'V/VO',6X,'G/VO*RP',3X,'F',9X,'WT/VO',
   -  5X,'WA/VO',6X,'PHI',6X,'VE/VO'/25X,'C',8X,'T/C',7X,'CL',8X,'CLI',
   -  7X,'CD',7X,'SIGCR')
120 FORMAT ('0',F8.3,F9.3,F11,5,F10.5,F9.4,F11.5,F10.5,F10.3,F10.3,/ ' ',
   -  20X,F8.3,F10.3,F9.5,F11.5,F10.6,F10.3)
121 FORMAT ('0','RPS='F10.2,5X,'RPM='F10.2,5X,'SHP='F10.2)
128 FORMAT(2I5)
129 FORMAT(I5,F5.1,2F7.3)
130 FORMAT(F6.4,3F8.5,F8.3,F8.5,F7.4,3F9.5)
131 FORMAT('0',4X,'XM',6X,'GM')
132 FORMAT(' ',F8.4,F9.5)
133 FORMAT(F6.4,F8.5)
    READ(2,102) TITLE
    READ (2,100) NV,NDEL
    READ (2,101) (X(I),V(I),I=1,NV)
    READ (2,108) RT,RH,CTP,GOVH,YPEAK,GOGM,CORP
    READ(2,100)NCASE
    READ (2,109) (NB(I),J(I),RP(I),1=1,NCASE)
    READ(2,101) DUMMY
    DO 15 ICASE=1,NCASE
    WRITE (3,103) TITLE
    WRITE (3,104) (X(I),V(I),I=1,NV)
    WRITE (3,105)
    WRITE (3,106) RT,YPEAK
    WRITE (3,115) RH,GOVH
    WRITE (3,116) DTP,GOGM
    WRITE (3,117) CORP
    WRITE (3,118) ICASE,NB(ICASE),J(ICASE),RP(ICASE)
    WRITE(2,128) NDEL,NCASE
    WRITE(2,129) ICASE,NB(ICASE),J(ICASE),RP(ICASE)
    IPRNT=0
    DELY = 1.0/(NDEL-1)
    YR(1)=0.0
    NN=NDEL-1
    DO 2 I=2,NN
  2 YR(I)=YR(I-1) + DELY
    YR(NDEL)=1.0
    CALL SPFIT (NV,X,V,VSC,ELV,A,B,C)
    CALL GAMMG(NGAM,COVH,YPEAK,XX,YY,SG,ELG)
  4 XO=RH/RP(ICASE)
    FUNO=0.0
    CT=0.0
    CONJ=J(ICASE)/PI
    DO 5 I=1,NDEL
    CALL SLGET (NGAM,XX,YY,SG,ELG,YR(I),GPI   ,GP,GDP)
    GR(I)=GPI*GOGM
    XR(I)=(RH+YR(I)*(RP(ICASE)-RH))/(RP(ICASE))
    RR=YR(I)*(RP(ICASE)-RH)+RH
```

```
      CALL SPGET(NV,X,V,VSC,ELV,RR,VV,VP,VDP)
      CALL THRUS(CONJ,NB(ICASE),GR(I),XR(I),VV)
      FUN=(XR(I)/CONJ-WT)*GR(I)
      CT=CT+0.5*(FUN-FUNO)*(XR(I)-XO)+FUNO*(XR(I)-XO)
      FUNO=FUN
      XO=XR(I)
    5 CONTINUE
      CT=CT*(2.0NB(ICASE)/PI*(RP(ICASE)/RT)**2)
      IF (IPRINT) 55,55,56
   55 DIFF1=CTP-CT
      GOGMT=GOGM
      GOGM=GOGM+DIFF1/2.0
      IPRNT=1
      GO TO 4
   56 DIFF2=CTP-CT
      SLOPE=(DIFF1-DIFF2)/(GOGMT-GOGM)
      GOGMF=GOGM
      GOGM=GOGM-DIFF2/SLOPE
      IF (ABS(DIFF2)-.00001) 8,8,4
    8 GOGM=GOGMF
      WRITE (3,107) CT,GOGM
      IPRNT=0
      FUNC=0.0
      FUNO=0.0
      XO=RH/RP(ICASE)
      XH=XO
      DO 9 I=1,NDEL
      RR=YR(I)*(RP(ICASE)-RH)+RH
      CALL SPGET (NV,X,V,VSC,ELV,XR(I),VC(I),VP,VDP)
      CALL SLGET (NGAM,XX,YY,SG,ELG,YR(I),GR(I),GP,GDP)
      GP(I)=GR(I)*GOGM
      CALL THRUS(CONJ,NB(ICASE),GR(I),XR(I),VC(I))
      FUN=2.0*XR(I)*VC(I)/(VC(I)+F*WA)
      FUNC=FUNC+.5*(FUN-FUNO)*(XR(I)-XO)+FUNO*(XR(I)-XO)
      FUNO=FUN
      XO=XR(I)
      X2(I)=SQRT(XH*XH+FUNC)
    9 CONTINUE
      CALL SPFIT (NDEL,VC,X2,VSC,ELV,A,B,C)
      CALL SPGET (NSEL,VC,X2,VSC,ELV,VC(NDEL),XVP,VP,VDP)
      BINT=X2(NDEL)-VP*VC(NDEL)
      X2(NDEL)=VP*1.0+BINT
      VC(NDEL)=1.0
      CALL SPFIT (NDEL,X2,VC,VSC,ELV,A,B,C)
      DO 90 I=1,NDEL
      IF (XR(I)-X2(NDEL)) 88,88,89
   88 CALL SPGET (NDEL,X2,VC,VSC,ELV,XR(I),A(I),VP,VDP)
      GO TO 90
   89 A(I)=1.0
   90 CONTINUE
      DO 91 I=1,NDEL
   91 VC(I)=A(I)
   10 FUNO=0.0
```

```
      XO=RH/RP(ICASE)
      CT=0.0
      DO 11 I=1,NDEL
      CALL SLGET(NGAM,XX,YY,SG,ELG,YR(I),GR(I),GP,GDP)
      GR(I)=GR(I)*GOGM
      CALL THRUS (CONJ,NB(ICASE),GR(I),XR(I),VC(I))
      CHORD=CORP*(RP(ICASE)-RH)
      CL=2.0*GR(I)/(CHORD*VE/RP(ICASE))
      TOC=(0.09-(0.03*YR(I)))*100.0
      CLI=CL/((100.0-TOC**1.35)*0.01)
      CALL CDFUN(CLI,TOC,CD)
      FUN=(XR(I)/CONJ-WT)*GR(I)*(1.0-CD/CL*SIN(PHI)/COS(PHI))
      CT=CT+0.5*(FUN-FUNO)*(XR(I)-XO)+FUNO*(XR(I)-XO)
      FUNO=FUN
      XO=XR(I)
   11 CONTINUE
      CT=CT*(2.0*NB(ICASE)/PI)*(RP(ICASE)/RT**2
      IF (IPRNT) 25,25,26
   25 DIFF1=CTP-CT
      GOGMT=GOGM
      GOGM=GOGM+DIFF1/2.0
      IPRNT=1
      GO to 10
   26 DIFF2=CTP-CT
      SLOPE=(DIFF1-DIFF2)/(GOGMT-GOGM)
      GOGMF=GOGM
      GOGM=GOGM-DIFF2/SLOPE
      DIFF1=DIFF2
      GOGMT=GOGMF
      IF (ABS(DIFF2)-.00001) 12,12,10
   12 GOGM=GOGMF
      IPRNT=0
      WRITE(3,110) CT,GOGM
      WRITE (3,119)
      CP=0.0
      FUNO=0.0
      XO=RH/RP(ICASE)
      DO 14 I=1,NDEL
      CALL SLGET(NGAM,XX,YY,DG,ELG,YR(I),GR(I),GP,GDP)
      GR(I)=GR(I)*GOGM
      CALL THRUS(CONJ,NB(ICASE),GR(I),XR(I),VC(I))
      CHORD=CORP*(RP(ICASE)-RH)
      CL=2.0*GR(I)/(CHORD*VE/RP(ICASE))
      TOC=(0.09-(0.03*YR(I)))*100.0
      CLI=CL/((100.0-TOC**1.35)*0.01)
      CALL CDFUN (CLI,TOC,CD)
      FUN=XR(I)*(VC(I)+WA)*GR(I)*(1.0+CD/CL*COS(PHI)/SIN(PHI))
      CP=CP+0.5*(FUN-FUNO)*(XR(I)-XO)+FUNO*(XR(I)-XO)
      XO=XR(I)
      FUNO=FUN
      SIGCR=(2.52*(TOC/100.0)+0.62*CLI)*VE**2
      PHII=PHI*57.29578
      WRITE(2,130) XR(I),GR(I),WT,WA,PHII,VE,CHORD,CL,CLI,VC(I)
      IF (NDEL-10) 46,46,43
```

```
      CALL SPGET(NV,X,V,VSC,ELV,RR,VV,VP,VDP)
      CALL THRUS(CONJ,NB(ICASE),GR(I),XR(I),VV)
      FUN=(XR(I)/CONJ-WT)*GR(I)
      CT=CT+0.5*(FUN-FUNO)*(XR(I)-XO)+FUNO*(XR(I)-XO)
      FUNO=FUN
      XO=XR(I)
    5 CONTINUE
      CT=CT*(2.0NB(ICASE)/PI*(RP(ICASE)/RT)**2)
      IF (IPRINT) 55,55,56
   55 DIFF1=CTP-CT
      GOGMT=GOGM
      GOGM=GOGM+DIFF1/2.0
      IPRNT=1
      GO TO 4
   56 DIFF2=CTP-CT
      SLOPE=(DIFF1-DIFF2)/(GOGMT-GOGM)
      GOGMF=GOGM
      GOGM=GOGM-DIFF2/SLOPE
      IF (ABS(DIFF2)-.00001) 8,8,4
    8 GOGM=GOGMF
      WRITE (3,107) CT,GOGM
      IPRNT=0
      FUNC=0.0
      FUNO=0.0
      XO=RH/RP(ICASE)
      XH=XO
      DO 9 I=1,NDEL
      RR=YR(I)*(RP(ICASE)-RH)+RH
      CALL SPGET (NV,X,V,VSC,ELV,XR(I),VC(I),VP,VDP)
      CALL SLGET (NGAM,XX,YY,SG,ELG,YR(I),GR(I),GP,GDP)
      GP(I)=GR(I)*GOGM
      CALL THRUS(CONJ,NB(ICASE),GR(I),XR(I),VC(I))
      FUN=2.0*XR(I)*VC(I)/(VC(I)+F*WA)
      FUNC=FUNC+.5*(FUN-FUNO)*(XR(I)-XO)+FUNO*(XR(I)-XO)
      FUNO=FUN
      XO=XR(I)
      X2(I)=SQRT(XH*XH+FUNC)
    9 CONTINUE
      CALL SPFIT (NDEL,VC,X2,VSC,ELV,A,B,C)
      CALL SPGET (NSEL,VC,X2,VSC,ELV,VC(NDEL),XVP,VP,VDP)
      BINT=X2(NDEL)-VP*VC(NDEL)
      X2(NDEL)=VP*1.0+BINT
      VC(NDEL)=1.0
      CALL SPFIT (NDEL,X2,VC,VSC,ELV,A,B,C)
      DO 90 I=1,NDEL
      IF (XR(I)-X2(NDEL)) 88,88,89
   88 CALL SPGET (NDEL,X2,VC,VSC,ELV,XR(I),A(I),VP,VDP)
      GO TO 90
   89 A(I)=1.0
   90 CONTINUE
      DO 91 I=1,NDEL
   91 VC(I)=A(I)
   10 FUNO=0.0
```

```
      XO=RH/RP(ICASE)
      CT=0.0
      DO 11 I=1,NDEL
      CALL SLGET(NGAM,XX,YY,SG,ELG,YR(I),GR(I),GP,GDP)
      GR(I)=GR(I)*GOGM
      CALL THRUS (CONJ,NB(ICASE),GR(I),XR(I),VC(I))
      CHORD=CORP*(RP(ICASE)-RH)
      CL=2.0*GR(I)/(CHORD*VE/RP(ICASE))
      TOC=(0.09-(0.03*YR(I)))*100.0
      CLI=CL/((100.0-TOC**1.35)*0.01)
      CALL CDFUN(CLI,TOC,CD)
      FUN=(XR(I)/CONJ-WT)*GR(I)*(1.0-CD/CL*SIN(PHI)/COS(PHI))
      CT=CT+0.5*(FUN-FUNO)*(XR(I)-XO)+FUNO*(XR(I)-XO)
      FUNO=FUN
      XO=XR(I)
   11 CONTINUE
      CT=CT*(2.0*NB(ICASE)/PI)*(RP(ICASE)/RT**2
      IF (IPRNT) 25,25,26
   25 DIFF1=CTP-CT
      GOGMT=GOGM
      GOGM=GOGM+DIFF1/2.0
      IPRNT=1
      GO to 10
   26 DIFF2=CTP-CT
      SLOPE=(DIFF1-DIFF2)/(GOGMT-GOGM)
      GOGMF=GOGM
      GOGM=GOGM-DIFF2/SLOPE
      DIFF1=DIFF2
      GOGMT=GOGMF
      IF (ABS(DIFF2)-.00001) 12,12,10
   12 GOGM=GOGMF
      IPRNT=0
      WRITE(3,110) CT,GOGM
      WRITE (3,119)
      CP=0.0
      FUNO=0.0
      XO=RH/RP(ICASE)
      DO 14 I=1,NDEL
      CALL SLGET(NGAM,XX,YY,DG,ELG,YR(I),GR(I),GP,GDP)
      GR(I)=GR(I)*GOGM
      CALL THRUS(CONJ,NB(ICASE),GR(I),XR(I),VC(I))
      CHORD=CORP*(RP(ICASE)-RH)
      CL=2.0*GR(I)/(CHORD*VE/RP(ICASE))
      TOC=(0.09-(0.03*YR(I)))*100.0
      CLI=CL/((100.0-TOC**1.35)*0.01)
      CALL CDFUN (CLI,TOC,CD)
      FUN=XR(I)*(VC(I)+WA)*GR(I)*(1.0+CD/CL*COS(PHI)/SIN(PHI))
      CP=CP+0.5*(FUN-FUNO)*(XR(I)-XO)+FUNO*(XR(I)-XO)
      XO=XR(I)
      FUNO=FUN
      SIGCR=(2.52*(TOC/100.0)+0.62*CLI)*VE**2
      PHII=PHI*57.29578
      WRITE(2,130) XR(I),GR(I),WT,WA,PHII,VE,CHORD,CL,CLI,VC(I)
      IF (NDEL-10) 46,46,43
```

```
43 IF (I-1) 44,46,44
44 IF(I-NDEL) 45,45,45
45 IP=YR(I)*10.0+.05
   IF (IP=IPRNT) 47,46,46
46 WRITE(3,120)YR(I),XR(I),VC(I),GR(I),F,WT,WA,PHII,VE,CHORD,TOC,CL,CLI,
  -  CD,SIGCR
   IPRNT=IPRNT+1
47 CONTINUE
14 CONTINUE
   CP=CP*2.0*NB(ICASE)/J(ICASE)*(RP(ICASE)/RT)**2
   ATA=CT/CP
   WRITE (3,112) CP,ATA
   DO 70 I=2,NDEL
   YR(I) = YR(I-1)+(DELY/2.0)
   CALL SLGET(NGAM,XX,YY,SG,ELG,YR(I),GR(I),GP,GDP)
   YM(I) = YR(I)
   XM(I) = (RH+YM(I)*(RP(ICASE)-RH))/(RP(ICASE))
   GRM(I) = GR(I)*GOGM
   WRITE(3,131)
70 CONTINUE
   STOP
   END
```

Appendix B

PROPELLER INTERFERENCE PROBLEM

Definition of FORTRAN Terms

AJ	advance ratio
ANS	sine of angle between free stream and tangent to body
BN	number of blades
BOUNH	subroutine that finds velocities at the hub induced by the bound vortex system
CHMN	mean chord
DDDH	θ' in Chapter IV, Equation (15)
DGAM	strength of free vortex system
DTH	value of θ that includes other blades
FREEH	subroutine that finds velocities at the hub induced by the free vortex system
GAMN	the mean strength of the bound vortex
GRM	the mean strength of the bound vortex
ISTART	index of starting section of the blade
IEND	last section of the blade
K	index of the inducing vortex section
N	index of the hub section where velocities are being induced
NCASE	number of cases being considered
NDEL	number of blade sections
NHUB	number of frustrums on the hub
PHI	hydrodynamics pitch angle
RP	radius of propeller
SUMAH	storage for numerical integration of axial induced velocity of free vortex system
THE	θ value for particular segment of free vorticity

THED	θ value of arc between two successive blades
THER	θ value for particular segment of free vorticity that includes contributions of other blades
THEDH	$\Delta\theta$ values for segment of free vorticity between 1/4 chord and 3/4 chord
VA	induced axial velocity at the hub
VR	induced radial velocity at the hub
VBA	induced axial velocity at the hub due to the bound vortex system
VBR	induced radial velocity in the hub due to the bound vortex system
VABAR	average induced axial velocity over the arc of the frustrum
VRBAR	average induced radial velocity over the arc of the frustrum
VFAH	induced axial velocity due to an entire segment of free vorticity
VFRH	induced radial velocity due to an entire segment of free vorticity
XH	axial position of hub frustrum
XHK	radial position of hub frustrum
XMK	mean radial position of vorticity
XMN	mean radial position of control point
XPQ	axial position of the 1/4 chord point of the propeller
XRN	radial position of vorticity
XX	distance along the chord of the free vortex segment
YH	radial position of hub
Z	distance between 1/4 chord position of the propeller and the frustum

FORTRAN PROGRAM LISTING

```
      SUBROUTINE FREEH(DGAM1,DGAM2,XRN,XRN1,THE,THED,XHK,XX,SINPHI,TANPHI,
     -  Z,VFALL,VFRLL)
      DATA PI/3.1415927/
      COSTHE=COS(THED)
      A11=((XRN1**2.0)-(2.0*XRN1*XHK*COSTHE)+(XHK**2.0)+(Z+XX*SINPHI)
     -  *(Z+XX*SINPHI))**1.5
      B11=((XRN **2.0)-(2.0*XRN *XHK*COSTHE)+(XHK**2.0)+(Z+XX*SINPHI)
     -  *(Z+XX*SINPHI))**1.5
      AA1=((XRN1*(XRN1-(XHK*COSTHE)))*(DGAM1/(4.0*PI)))/A11
      BB1=((XRN *(XRN -(XHK*COSTHE)))*(DGAM2/(4.0*PI)))/B11
      VFALL=AA1+BB1
      AAA=(DGAM1/(4.0*PI))*XRN1*((TANPHI*SIN(THED)* XRN1)-(COSTHE*
     -  (Z+XX*SINPHI)))/A11
      BBB=(DGAM2/(4.0*PI))*XRN *((TANPH1*SIN(THED)* XRN )-(COSTHE*
     -  (Z+XX*SINPHI)))/B11
      VFRLL=AAA+BBB
      RETURN
      END
      SUBROUTINE BOUNH(DTH,XHK,XMN,Z,XRN,XRN1,GAMN,VBA,VBR)
      DATA PI/3.1415927/
      COSDTH=COS(DTH)
      A1=XHK*XHK*SIN(DTH)*SIN(DTH)+Z*Z
      A2=SQRT((XRN**2.0)-(2.0*XRN*XHK*COSTH)+XHK**2.0+Z*Z)
      AA=(XRN-(XHK*COSDTH))/(A1*A2)
      B2=SQRT((XRN1**2.0)-(2.0*XRN1*XHK*COSDTH)+XHK**2.0+Z*Z)
      BB=(XRN1-(XHK*COSDTH))/(A1*B2)
      VBA=-((XHK*GAMN*SIN(DTH))/(4.0*PI))*(AA-BB)
      VRB=-((Z*SIN(DTH)*GAMN)/(4.0*PI))*(AA-BB)
      RETURN
      END
      DIMENSION XR(22),GR(22),WT(22),WA(22),PHI(22),CHORD(22),CL(22),CLI(22),
     -  VC(22),XM(22),GRM(22),TITLE(20),VE(22),XH(50),YH(50)
      DIMENSION VN(50)
      DATA PI/3.1415927/
  100 FORMAT(20A4)
  101 FORMAT(3I5)
  102 FORMAT(I5,F5.1,3F7.3)
  103 FORMAT(F6.4,3F8.5,F8.3,F8.5,F7.4,3F9.5)
  104 FORMAT(F6.4,F8.5)
  105 FORMAT('1',20A4)
  106 FORMAT('0','CASE=',I2,5X,'B=',F5.1,5X'J=',F7.3,5X,'RP=',F7.3,4X,'
     1XPQ=',F7.3)
  107 FORMAT('0',4X,'X',5X,'G/VO*RP',3X,'WT/VO',4X,'WA/VO',4X,'PHI',4X,
     2   'VE/VO',4X,'C',7X,'CL',7X,'CLI',6X,'VVO')
  108 FORMAT('  ',F8.4,3F9.5,F8.3,F8.5,F7.4,2F9.5,F9.6)
  109 FORMAT('0',4X,'XM',6X,'GM')
  110 FORMAT(' ',F8.4,F9.5)
  114 FORMAT(1X,2F10.5)
  115 FORMAT('0',4X,'XHUB',7X,'YHUB')
  116 FORMAT('0',VABAR=',F8.5,4X,'VRBAR=',F8.5,4X,'VN=',F8.5)
  118 FORMAT(2F10.5)
```

```
119 FORMAT(3F10.5)
    READ(2.100) TITLE
    READ(2,101) NDEL,NCASE,NHUB
    READ(2,102) ISTART,BN,AJ,RP,XPQ
    READ(2,103)(XR(I),GR(I),WT(I),WA(I),PHI(I),VE(I),CHORD(I),CL(I),CLI(I),
   -  VC(I),VC(I),I=1,NDEL)
    READ(2,104) (XM(I),GRM(I),I=2,NDEL)
    READ(2,118)(XH(I),YH(I),I=1,NHUB)
    NB = BN
    DO 15 ICASE=1,NCASE
    WRITE(3,105) TITLE
    WRITE(3,106) ICASE,BN,AJ,RP,XPQ
    WRITE(3,107)
    DO 10 I=1,NDEL
 10 WRITE(3,108) XR(I),GR(I),WT(I),WA(I),PHI(I),VE(I),CHORD(I),CL(I),
   2  CLI(I),VC(I)
    WRITE(3,109)
    DO 11 I=2,NDEL
 11 WRITE(3,110) XM(I),GRM(I)
    WRITE(3,115)
    DO 33 I=1,NHUB
 33 WRITE(3,114) XH(I),YH(I)
    DO 34 I=1,NHUB
    XH(I) = XH(I)/RP
 34 YH(I) = YH(I)/RP
    XPQ = XPQ/RP
    IEND = NHUB-1
    DO 12 K=ISTART,IEND
    VR = 0.0
    VA = 0.0
    DDTH = 0.0
    Z = XPQ-XH(K)
    XHK=YH(K)
    THED = (2.0*PI)/(BN*10.0)
    DO 16 LL=1,10
    DDTH = DDTH+THED
    VBAH = 0.0
    VBRH = 0.0
    VFAH = 0.0
    VFRH = 0.0
    DO 13 N=2,NDEL
    CHMN = (CHORD(N)+CHORD(N-1))/2.0
    PHIMN = ((PHI(N)+PHI(N-1))/2.0)/57.29578
    SINPHI=SIN(PHIMN)
    TANPHI=SINPHI/COS(PHIMN)
    XMN = XM(N)
    GAMN = GRM(N)
    DO 14 L=1,NB
    DTH = DDTH+((2.0*PI)*(L-1))-BN
    CALL BOUNH(DTH,XHK,XMN,Z,XR(N),XR(N-1),GAMN,VBA,VBR)
    VBRH = VBRH+VBR
    VBAH = VBAH+VBA
 14 CONTINUE
    DGAM1 = GAMN-GR(N-1)
    DGAM2 = GR(N)-GAMN
```

```
64 SUMAH = 0.0
   SUMRH = 0.0
   VFALL = 0.0
   VFRLL = 0.0
   VFAHL = 0.0
   VFRHL = 0.0
   DDDH = DDTH-(CHMN*COS(PHIMN))/(2.0*XMN*RP)
   DX = CHMN/(40.0*RP)
   DO 20 L=1,NB
   DBL = ((2.0*PI)*(L-1))/BN
   XX = 0.0
   THEDH = DDH/20.0
   THE = 0.0
   THEO = 0.0
   DO 22 LB=1,21
   THER = THE+DBL
   CALL FREEH(DGAM1,DGAM2,XR(N),XR(N-1),THE,THER,XHK,XX,SINPHI,TANPHI,Z,
  -  VFALL,VFRLL)
   SUMAH = SUMAH+0.5*(VFALL-VFAHL)*(THE-THEO)+(VFAHL)*(THE-THEO)
   SUMRH = SUMRH+0.5*(VFRLL-VFRHL)*(THE-THEO)+(VFRHL)*(THE-THEO)
   VFAHL = VFALL
   VFRHL = VFRLL
   THEO = THE
   XX = XX+DX
22 THE = THEO+THEDH
   VFAH = VFAH+SUMAH
   VFRH = VFRH+SUMRH
20 CONTINUE
13 CONTINUE
   VA = VA+VBA+VFAH
16 VR = VR+VFRH+VBRH
   VRBAR = VR/10.
   VABAR = VA/10.
   DELX = XH(K+1)-XH(K)
   DELY = YH(K+1)-YH(K)
   DELS = SQRT(DELX*DELX+DELY*DELY)
   ANS = DELY/DELS
   ANC = DELX/DELS
   VN(K) = VRBAR*ANC+VABAR*ANS
12 WRITE(3,116) VABAR,VRBAR,VN(K)
15 CONTINUE
   DO 17 I=ISTART,IEND
   XH(I) = XH(K)*RP
   YH(I) = YH(I)*RP
17 WRITE(7,119)  XH(I),YH(I)
   STOP
   END
```

Description of FORTRAN Program

This program applies the method developed in Chapter IV for the calculation of normal velocity on the hub induced by the propeller vortex system. The program begins by reading in an 80-character title, the number of divisions on the blade, the number of cases to be considered and the number of points specified on the hub. The next card read contains information on the number of blades, the radius of the propeller in inches, the advance ratio and the axial position of the 1/4 chord point. The next two groups of cards read the punched output of the lifting line design program shown in Appendix A. The final group of data to be read in are the coordinates of the hub. It is at these points that the normal velocity is calculated.

Once the data has been read, the program writes the data before starting the calculations, and then normalizes the hub coordinates with respect to the radius of the propeller. The program then enters a loop so that it starts to consider the stations of the hub one at a time. The axial distance between the bound vortex system and the hub station is then found along with the angle θ between two successive blades. This angle is further divided into 10 subsegments where the normal velocity will be calculated. After initializing some variables used for summation, another loop is entered that considers the segments of vorticity along the blade. The induced value of velocity caused by the bound vortex system is then calculated in subroutine BOUNH for each of the seven blades. This subroutine represents Equation (19) and (20) in Chapter IV. The program next considers the induced velocity due to the free vorticity. The free vortex which extends from the 1/4 to 3/4 chord points is divided into 20 segments so that the velocity can be found by numerical integration.

Subroutine FREEH calculates the values of the integral and represents Equation (60) and (61) in Chapter IV. As in the bound vortex system, this induced velocity is calculated for the other blades as well. Once both the velocities induced by the bound and free segments of vorticity are known, they are summed and the next segment of vorticity is considered. After all the segments of vorticity are dealt with, the next point on the arc of the hub is calculated and the entire procedure is repeated. Once the values of induced velocity are known over these 10 small arcs, the average velocity is calculated. This velocity is then used with the sine and cosine of the angle between the tangent to the surface of the hub and the free stream to find the normal component of velocity. After this value is known for each of the hub stations, the coordinates of the hub and its normal induced velocity are punched out on cards. Approximate running time of this program with 31 hub stations on the IBM 370/168 is 450 seconds.

Appendix C

A.M.O. SMITH AND J. PIERCE SOLUTION OF THE NEUMAN PROBLEM

FORTRAN PROGRAM LISTING

```
      DIMENSION TITLE (20),VN(200)
      DIMENSION X(200),XPP(200),YPP(200),ANS(200),COED(200,200)
1     FORMAT (2(I4,F4.1)
    2 FORMAT (3F10.5)
3     FORMAT(10X,I3,2X,F10.5,5X,F10.5,4(3X,E14.7))
4     FORMAT(I3,3X,I3,3X,E14.7,3X,E14.7)
5     FORMAT(I3,3Z,I3,3X,E14.7)
    6 FORMAT (20A4)
1000  FORMAT ('0',20A4)
7     FORMAT(10X,'NUM',6X,'XP',13X,'YP',12X,'VTAN',14X,'CP',14X,'VNOR',1
     13X,'SIGMA'//)
8     FORMAT(1X,'PRESSURE DISTRIBUTION FROM AMO SMITH REPORT')
9     FORMAT(2F10,5,E14.7)
      LUKE=+1.0
      LAKE=+1.0

      LAKE AND LUKE MUST EQUAL MINUS ONE FOR A PRINT OUT OF INTERMEDIATE
      MATRIX
      WRITE(6,8)
      READ(5,6,END=59) TITLE
      WRITE (6,1000) TITLE
      WRITE(6,1001)
1001  FORMAT('-',2X,'SEG',11X,'X',15X,'Y",16X,'XP',15X,'YP',16X,'DELS')


      N=NUMBER OF POINTS FOR FIRST BODY
      HAR=+1(EXTERNAL FLOW ON FIRST BODY)
      HAR=-1(INTERNAL FLOW ON FIRST BODY)
      LOW=NUMBER OF POINTS FOR SECOND BODY)
      HUB=+1(EXTERNAL FLOW ON SECOND BODY)
      HUG=-1(INTERNAL FLOW ON SECOND BODY)


      READ(5,1) N,HAR,LOW,HUG

      NM=NUMBER OF SEGMENTS ON FIRST BODY

      NM=N-1
      NA=N+LOW
      DO 10 I=1,NA
   10 READ(5,2) X(I),Y(I),VN(I)
      NAAA=NA
      IF(LOW-0) 811,810,811
```

```
      NA=TOTAL NUMBER OF SEGMENTS
  810 NA=NA-1
      GO TO 809
  811 NA=NA-2
  809 DO 501 LOIS=1,NA
      IF(LOIS-NM) 800,800,801
  800 I=LOIS
      H=HAR
      GO TO 802
  801 I=LOIS+1
      H=HUB
  802 DELX=X(I+1)-X(I)
      DELY=Y(I+1)=Y(I)
      DELS=SQRT(DELX*DELX+DELY*DELY)
      ANS(LOIS)=DELY/DELS
      BEE=DELX/DELS
      XP=(X(I+1)+X(I))/2.
      YP=(Y(I+1)+Y(I))/2.
      WRITE(6,2001) LOIS,X(I),Y(I),XP,YP,DELS
 2001 FORMAT(' ',I5,5(E18.5))
      XPP(LOIS)=XP
      YPP(LOIS)=YP
      DO 701 LEW=1,NA
      IF(LEW-NM) 803,803,804
  803 J=LEW
      GO TO 805
  804 J=LEW+1
  805 IF (I-J) 502,11,502
  502 AMIN=X(J)-XP
      BMIN=XP-X(J+1)
      AMIN=ABS(AMIN)
      BMIN=ABS(BMIN)
      IF (AMIN-BMIN) 920,920,503
  920 DMIN=AMIN
      GO TO 504
  503 DMIN=BMIN
  504 JANE=1
      GO TO 12
   11 JANE=2
   12 IF (YP-Y(J)) 900,901,900
  901 IF (YP-Y(J+1)) 900,902,900
  902 B=1.0
      XT=0.0
      YT=0.0
      JOHN=J+1
      DO 903 K=J,JOHN
      S=X(K)
      ETA=Y(K)
      CAY=4.0*ETA*YP/((YP+ETA)*(YP+ETA)+(XP-S)*(XP-S))
      C=1.0-CAY
      IF(C-0.0) 333,334,336
  333 CC=ABS(C)
      GO TO 335
```

```
 334 CC=.111E-37
     GO TO 335
 336 CC=C
 335 E1=1.3862944+.1119723*C+.0725296*C*C
     E1=E1-(.5+.1213478*C+.0288729*C*C)*ALOG(CC)
     AX=YP*SQRT ((XP-S)*(XP-S)+(YP+ETA)*(YP+ETA)
     AX=B*2.0*ETA*(EP-S)*E1/AX
     YT=YT-AX
     AX=SQRT ((XP-S)*(XP-S)+(YP+ETA)*(YP+ETA))
     XT=B*4.0*ETA*E1/AX+XT
 903 B=-1.0
     GO TO 702
 900 DELX=X(J+1)-X(J)
     DELY=Y(J+1)-Y(J)
     DELS=SQRT (DELX*DELX+DELY*DELY)
     GO TO (13,14),JANE
  13 AN=16.0*DELS/DMIN
     HAN=0.0
     JOHN=1
     DO 505 K=1.32
     HAN=HAN+2.0
     JOHN=JOHN+2
     IF(AN-HAN) 506,506,505
 505 CONTINUE
 506 DELS=DELS/HAN
     DELX=DELX/HAN
     DELY=DELY/HAN
     GO TO 15
  14 DELS=DELS/32.
     DELX=DELX/32.
     DELY=DELY/32.
  15 GO TO (16,17),JANE
  17 JOHN=15
  16 JACK=1
     S=X(J)
     ETA=Y(J)
     XT=0.0
     YT=0.0
     B=1.0
 512 DO 507 K=JACK,JOHN
     CAY=4.*ETA*YP/((YP+ETA)*(YP+ETA)+(XP-S)*(XP-S)
     C=1.0-CAY
     IF(C-0.0) 381,382,889
 381 CC=ABS(C)
     GO TO 83
 382 CC=.111E-31
     GO TO 83
 889 CC=C
  83 E1=1.3862944+.1119723*C+.0725296*C*C
     E1=E1-(.5+.1213478*C+.0288729*C*C)*ALOG(CC)
     E2=E2-(.2452727*C+.01412496*C*C)*ALOG(CC)
     AX=ETA*(XP-S)*E2/SQRT ((YP+ETA)*(YP+ETA)+(XP-S)*(XP-S))
     AX=AX/((YP-ETA)*(YP-ETA)+(XP-S)*(XP-S))
```

```
      AY=ETA/(YP*SQRT ((YP+ETA)*(YP+ETA)+(XP-S)*(XP-S)))
      AZ=YP*YP-ETA*ETA-(XP-S)*(XP-S)
      AZ=AZ/((YP-ETA)*(YP-ETA)+(XP-S)*(XP-S))
      XT=XT-4.0*B*AX*DELS/3.0
      YT=YT-2.0*B*AY*(E1+AZ*E2)*DELS/3.0
      IF (B-4.0) 508,509,509
  509 B=2.0
      L=JOHN-K-1
      IF (L) 510,510,511
  510 B=1.0
      GO TO 511
  508 B=4.0
  511 S=S+DELX
      ETA=ETA+DELY
  507 CONTINUE
      GO TO (702,19),JANE
   19 S=S-DELX
      ETA=ETA-DELY
      IF (JOHN-17) 602,603,604
  602 JACK=15
      JOHN=17
      DELS=.75*DELS
      DELX=.75*DELX
      DELY=.75*DELY
      B=1.0
      GO TO 512
  603 S=S+1.333333*DELX
      ETA=ETA+1.333333*DELY
      JACK=17
      JOHN=19
      B=1.0
      GO TO 512
  604 IF (JOHN-28) 605,605,606
  605 JACK-19
      JOHN=33
      B=1.0
      DELS=DELS/.75
      DELX=DELX/.75
      DELY=DELY/.75
      GO TO 512
  606 T=DELS/(2.*YP)
      A=DELX/DELS
      D=DELY/DELS
      XII=13.0/72.0+1.0/12.0*(ALOG(T/8.0)+D*D)
      XII=A*D*(2.0*T+XII*T*T*T)
      YII=3.+3.*(ALOG(T/8.0)-D*D)-2.0*D*D*D
      YII=(2.0*D*D+2.0*ALOG(T/8.0))*T-1.0/24.0*YII*T*T*T
      XT=XT+XII
      YT=YT+YII
  702 WRITE(9) XT,YT
      COED(LOIS,LEW)=BEE*YT-ANS(LOIS)*XT
      IF(LOIS-LEW) 22,21,22
   21 COEF(LOIS,LEW)+COED(LOIS,LEW)-H*6.28318
```

```
 22   IF(LAKE)703,20,20
703   WRITE(6,4)LOIS,LEW,XT,YT
 20   IF(LUKE) 23,701,701
 23   WRITE(6,5) LOIS,LEW,COED(LOIS,LEW)
 701  CONTINUE
 501  CONTINUE
      WRITE(6,2002) X(NAAA),Y(NAAA)
 2002 FORMAT(' ',5X,2(E18.5))
      M=NA
      K=1
      DO 698 I=1,NA
 698  ANS(I)=ANS(I)+VN(I)
 51   DO 52 I=K,M
      IF(COED(I,K)) 53,52,53
 53   B=COED(I,K)
      ANS(I)=ANS(I)/B
      DO 92 J=K,NA
 92   COED(I,J)=COED(I,J)/B
 52   CONTINUE
      MAN=K
 56   IF(COED(K,K)) 54,55,54
 54   L=K+1
      IF(K-M) 57,58,59
 57   DO 60 I=L,M
      IF(COED(I,K))61,60,61
 61   ANS(I)=ANS(I)-ANS(K)
      DO 90 J=K,NA
 90   COED(I,J)=COED(I,J)-COED(K,J)
 60   CONTINUE
      GO TO 63
 55   MAN=MAN+1
      IF(MAN-M) 64,64,59
 64   DO 66 J=K,NA
 66   COED(K,J)=COED(K,J)+COED(MAN,J)
      ANS(K)=ANS(K)+ANS(MAN)
      GO TO 56
 63   K=K+1
      IF(M-K) 58,51,51
 58   K=NA
 70   B=0.0
      IF(K)71,71,72
 72   I=K
 76   I=I+1
      IF(NA-I) 73,74,74
 74   B=B+COED(K,I)*COED(I,I)
      GO TO 76
 73   COED(K,K)=ANS(K)-B
      K=K-1
      GO TO 70
 71   WRITE(6,7)
      ENDFILE 9
      REWIND 9
      WRITE (7,6) TITLE
```

```
      NZ=N+LOW
      WRITE(7,2) X(N),X(NZ)
      WRITE(7,610) N,LOW
610   FORMAT(I4,4X,I4)
      DO 30 LOIS=1,NA
      IF(LOIS-NM) 905,905,906
905   I=LOIS
      H=HAR
      GO TO 907
906   I=LOIS+1
      H=HUG
907   DELX=X(I+1)-X(I)
      DELY=Y(I+1)-Y(I)
      DELS=SQRT(DELX**2+DELY**2)
      A=DELY/DELS
      B=DELX/DELS



      U=1.0
      V=0.0
      DO 31 J=1,NA
      READ(9) XT,YT
      U=U+COED(J,J)*XT
31    V=V+COED(J,J)*YT
      VTAN=U*B+B*A
      CP1=1.0-VTAN**2
      VNOR=V*B-U*A-H*6.28318*COED(LOIS,LOIS)
      WRITE(6,3) LOIS,XPP(LOIS),YPP(LOIS),VTAN,CP1,VNOR,COED(LOIS,LOIS)
      WRITE(7,9) XPP(LOIS),YPP(LOIS),COED(LOIS,LOIS)
30    CONTINUE
59    STOP
      END
```

A description of variables and the program will be found in Appendices G and H of Reference 10.

Appendix D

PROPELLER DESIGN PROGRAM

Definition of FORTRAN Terms

AJ	advance ratio
ALAM	value of middle equation on page 12 of Reference 12
BN	number of blades
CHMK	mean chord at point of vorticity
CHMN	mean chord at control point
CLI	design lift coefficient from lifting line design program
CLILS	design lift coefficient from lifting line surface
DDTH	θ value for 1/4 of chord
DELZM	change in camber due to thickness
DGAM	strength of free vorticity
DTH	θ value of vorticity of 1/4 chord taking into account other blades
DA	axial distance from 1/4 chord point
DUKH	change in induced velocity at the 1/2 chord point from Equation (64) in Chapter V
DUKQ	change in induced velocity at the 3/4 chord point from Equation (63) in Chapter V
GAMN	mean strength of bound vorticity between two points
GMH	angle made by induced velocity at the 1/2 chord point
GMQ	angle made by induced velocity at the 3/4 chord point
GMW	angle made by the induced velocity of the lifting line
K	index of points of vorticity
N	index of control points
PHI	hydrodynamic pitch angle from lifting line program

RP	radius of the propeller
SLOPE	$\frac{df}{dx}$ in Equation (63) of Chapter V
SUMTH, SUMTA	summation of numerical integration of tangential velocity induced by the free vortex system at the 1/2 chord and 3/4 chord points
SUMAH, SUMAQ	axial components of above
THE	θ value for particular segment of free vorticity
THEDH, THEDQ	$\Delta\theta$ values for numerical integration of free vorticity up to the 1/2 chord point and up to the 3/4 chord point
UKH	velocity induced at the 1/2 chord control point by the entire lifting surface
UKQ	velocity induced at the 3/4 chord control point by the entire lifting surface
VBA, VBT	axial and tangential components of velocity induced by a segment of the bound vortex system
VBAH, VBTH	axial and tangential components of velocity induced by the entire bound vortex system at the 1/2 chord point
VBAQ, VBTQ	same as the above at the 3/4 chord point
VC	normalized velocity in the wake
VFAH, VFTH	axial and tangential components of velocity induced by the free vortex system
VFAQ, VFTQ	same as the above at the 3/4 chord point
VHAH, VHAQ	velocity induced by the hub and body at the 1/2 and 3/4 control points
WT, WA	tangential and axial components of induced velocity due to the lifting line
XM, XMK, XMN	mean radial stations along blade for vorticity and the control point
XR	normalized radial position along the blade
XRN	normalized radial position along the blade of the control point
ZMKLL	maximum camber of the lifting line

ZMKLS maximum camber of the lifting surface

ZMKSC maximum camber of the lifting surface circular arc

The definition of terms in subroutine VELO are given in Appendix H of Reference 10.

FORTRAN PROGRAM LISTING

```
      SUBROUTINE BOUN(DTH,DDTH,XMK,XMN,TANPHI,XRN,XRN1,GAMN,VBA,VBT)
      DATA PI/3.1415927/
      COSDTH=COS(DTH)
      A1=(XMK*XMK*SIN(DTH)*SIN(DTH))+((XMN*DDTH*TANPHI)**2.0)
      A2=SQRT((XRN**2.0)-(2.0*XRN*XMK*COSDTH)+(XMK**2.0)+(XMN*DDTH*TANPHI)
     -  **2.0)
      AA=(XRN-(XMK*COSTH))/(A1*A2)
      B2=SQRT((XRN1**2.0)-(2.0*XRN1*XMK*COSDTH)+(XMK**2.0)+(XMN*DDTH*TANPHI)
     -  **2.0)
      BB=(XRN1-(XMK*COSTH))/(A1*B2)
      VBA=-((XMK*GAMN*SIN(DTH))/(4.0*PI))*(AA-BB)
      VBT=((DDTH*GAMN*COSDTH*XMN*TANPHI)/(4.0*PI))*(AA-BB)
      RETURN
      END
      SUBROUTINE FREE(DGAM1,DGAM2,XRN,XRN1,THE,THED,XMK,TANPHI,VFALL,VFTLL)
      DATA PI/3.1415927/
      COSTHE=COS(THED)
      A11=((XRN1**2.0)-(2.0*XRN1*XMK*COSTHE)+(XMK**2.0)+((XRN1*THE*TANPHI)
     -  **2.0))**1.5
      B11=((XRN**2.0)-(2.0*XRN*XMK*COSTHE)+(XMK**2.0)+((XRN*THE*TANPHI)**
     -  2.0))**1.5
      AA1=((XRN1*(XRN1-(XMK*COSTHE)))*(DGAM1/(4.0*PI)))/A11
      BB1=((XRN *(XRN -(XMK*COSTHE)))*(DGAM2/(4.0*PI)))/B11
      VFALL=AA1+BB1
      AAA=((XMK-XRN1*(COSTHE+THE*SIN(THED)))*(DGAM1*XRN1*TANPHI/(4.0*PI)))
     -  /A11
      BBB=((XMK-XRN *(COSTHE+THE*SIN(THED)))*(DGAM2*XRN *TANPHI/(4.0*PI)))
     -  /B11
      VFTLL=AAA+BBB
      RETURN
      END
      SUBROUTINE VELO
      DIMENSION X(80),Y(80),SIG(80)
  100 FORMAT (I4)
  101 FORMAT(2F10,5,E14.7)
  102 FORMAT('0',E12.5)
      READ(2,100) N
      DO 1 I=1,N
    1 READ(2,101) X(I),Y(I),SIG(I)
      RETURN
      ENTRY CAVEL(XP,YP,U)
      U=0.0
      NA=N-1
      DO 701 J=1,NA
      DM1=(XP-X(J))*(XP-X(J))+(YP-Y(J))*(YP-Y(J))
      DM2=(XP-X(J+1))*(XP-X(J+L))+(YP-Y(J+1))*(YP-Y(J+L))
      IF(DM1-DM2) 502,502,503
  502 DMIN=SQRT(DM1)
      GO TO 504
```

```
503 DMIN=SQRT(DM2)
504 DELS=(X(J+L)-X(J))*(X(J+1)-X(J))
    DELS=DELS+(Y(J+1)-Y(J))*(Y(J+1)-Y(J))
    DELS=SQRT(DELS)
    AN=16*DELS/DMIN
    H=0.0
    JOHN=1
    DO 505 K=1,64
    H=H=2.0
    JOHN=JOHN+2
    IF(AN-H) 506,506,505
505 CONTINUE
506 DELS=DELS/H
    DELX=(X(J+1)-X(J))/H
    DELY=(Y(J+1)-Y(J))/H
    S=X(J)
    ETA=Y(J)
    JACK=1
    B=1.0
    XT=0.0
    YT=0.0
    DO 507 K=JACK,JOHN
    CAY=4.0*ETA*YP/((YP+ETA)*(YP+ETA)+(XP-S)*(XP-S))
    C=1.0-CAY
    IF(C) 381,382,889
381 CC=ABS(C)
    GO TO 83
382 CC=.11E-31
    GO TO 83
889 CC=C
 83 E2=1.+.4630151*C+.1077812*C*C
    E2=E2-(.2452727*C+.01412496*C*C)*ALOG(CC)
    AX=ETA*(XP-S)*E2/SQRT((YP+ETA)*(YP+ETA)+(XP-S)*(XP-S)
    AX=AX/((YP-ETA)*(YP-ETA)+(XP-S)*(XP-S))
    XT=XT-4.0*B*AX*DELS/3.0
    IF(B-4.0) 508,509,509
509 B=2.0
    L=JOHN-K-1
    IF(L) 510,510,511
510 B=1.0
    GO TO 511
508 B=4.0
511 S=S+DELX
    ETA=ETA+DELY
507 CONTINUE
    U=U+SIG(J)*XT
701 CONTINUE
    WRITE(3,102) U
    RETURN
    END
    DIMENSION XR(22),GR(22),WT(22),WA(22),PHI(22),CHORD(22),CL(22),CLI(22),
   -  VC(22),XM(22),GRM(22),TITLE(20),VE(22)
    DATA PI/3.1415927/
```

```
100 FORMAT(20A4)
101 FORMAT(2I5)
102 FORMAT(I5,F5.1,3F7.3)
103 FORMAT(F6.4,3F8.5,F8.3,F8.5,F7.4,3F9.5)
104 FORMAT(F6.4,F8.5)
105 FORMAT('1',20A4)
106 FORMAT('0','CASE='I2,5X,'B',F5.1,5X'J=',F7.3,5X,'RP=',F7.3,4X,'1XPQ=
   -  ',F7.3)
107 FORMAT('0',4X,'X',5X,'G/VO*RP',3X,'WT/VO',4X,'WA/VO',4X,'PHI',4X,
   2  'VE/VO',4X,'C',7X,'CL',7X,'CLI',6X,'VVO')
108 FORMAT(' ',F8.4,3F9.5,F8.3,F8.5,F7.4,2F9.5,F9.6)
109 FORMAT('0',4X,'XM',6X,'GM')
110 FORMAT(' ',F8.4,F9.5)
111 FORMAT('1',2X,'N',2X,'L',6X,'VBAH',5X,'VBTH',5X,'VBAQ',5X,'VBTQ',5X,
   -  'VFAH',5X,'VFTH',5X,'VFAQ',5X,'VFTQ')
112 FORMAT(' ',I6,2X,4F9.5)
113 FORMAT(' ',I6,3BX,4F9.5)
114 FORMAT(' ',I3,5X,8F9.5)
115 FORMAT('0','K=',I3,5X,'UAKH=',F9.5,5X,'UTKH=',F9.5,5X,'UAKQ=',F9.5
   -  , 5X,'UTKQ=',F9.5)
116 FORMAT('0','UH=',F8.5,4X,'UQ=',F8.5,4X,'GH=',F7.3,4X,'GQ=',F7.3,4X,
   -  'WT=',F8.5,4X,'WA='WA=',F8.5,4X,'W=',F8.5,4X,'GMW=',F7.3)
117 FORMAT('0','ALF=',F7.3,4X,'CLIS=',F8.4,4X,'CLI='F8.4,4X,'ZS=',F8.4,4X,
   -  'ZSC=',F8.4,4X,'DZ=',F8.4,4X,'ZL=',F8.4)
    READ(2,100 TITLE
    READ(2,101) NDEL NCASE
    READ(2,102) ISTART,BN,AJ,RP,XPQ
    READ(2,103)(XR(I),GR(I),WT(I),WA(I),PHI(I),VE(I),CHORD(I),CL(I),CLI(I),
   -  VC(I),I=1,NDEL)
    READ(2,104) (XM(I),GRM(I),I=2,NDEL)
    NB = BN
    DO 17 I=2,NDEL
    XM(I)=XM(I)*RP
 17 GRM(I)=GRM(I)*RP
    DO 18 I=1,NDEL
    XR(I)=XR(I)*RP
 18 GR(I)=GR(I)*RP
    DO 15 ICASE=1,NCASE
    WRITE(3,105) TITLE
    WRITE(3,106) ICASE,BN,AJ,RP,XPQ
    WRITE(3,107)
    DO 10 I=1,NDEL
 10 WRITE(3,108) XR(I),GR(I),WT(I),WA(I),PHI(I),VE(I),CHORD(I),CL(I),
   2  CLI(I),VC(I)
    WRITE(3,109)
    DO 11 I=2,NDEL
 11 WRITE(3,110) XM(I),GRM(I)
    CALL VELO
    DO 12 K=ISTART,NDEL
    VBAH=0.0
    VBTH=0.0
    VBAQ=0.0
    VBTQ=0.0
```

```
      VFAH=0.0
      VFTH=0.0
      VFAQ=0.0
      VFTQ=0.0
      CHMK = (CHORD(K)+CHORD(K-1)/2.0
      PHIMK = ((PHI(K)+PHI(K-1))/2.0)/57.29578
      XMK = XM(K)
      DQ = (CHMK/4.0)*SIN(PHIMK)
      XHH = XPQ+DQ
      XHQ = XHH+DQ
      CALL CAVEL(XHH,XMK,VHAH)
      CALL CAVEL(XHQ,XMK,VHAQ)
      GAMK = GRM(K)
      WRITE(3,111)
      DO 13 N=2,NDEL
      CHMN = (CHORD(N)+CHORD(N-1))/2.0
      PHIMN = ((PHI(N)+PHI(N-1))/2.0)/57.29578
      TANPHI=SIN(PHIMN)/COS(PHIMN)
      XMN = XM(N)
      GAMN = GRM(N)
      DO 14 L=1,NB
      DDTH = (CHMN*COS(PHIMN))/(4.0*XMN)
      DTH = DDTH+((2.0*PI)*(L-1))/BN
      CALL BOUN(DTH,DDTH,XMK,XMN,TANPHI,XR(N),XR(N-1),
     1GAMN,VBA,VBT)
      VBAH = VBAH+VBA
      VBTH = VBTH+VBT
      DDTH = DDTH+((CHMK*COS(PHIMK))/(4.0*XMK))
      DTH = DDTH+((2.0*PI)*(L-1))/BN
      CALL BOUN(DTH,DDTH,XMK,XMN,TANPHI,XR(N),XR(N-1),
     1GAMN,VBA,VBT)
      VBAQ = VBAQ+VBA
      VBTQ = VBTQ+VBT
   14 CONTINUE
      WRITE(3,112)N,VBAH,VBTH,VBAQ,VBTQ
      DGAM1 = GAMN-GR(N-1)
      DGAM2 = GR(N)-GAMN
   64 SUMAH = 0.0
      SUMTH = 0.0
      SUMAQ = 0.0
      SUMTQ = 0.0
      VFAHL = 0.0
      VFTHL = 0.0
      VFAQL = 0.0
      VFTQL = 0.0
      VFTLL = 0.0
      VFALL = 0.0
      DO 20 L=1,NB
      DDTH = (CHMN*COS(PHIMN))/(4.0*XMN)
      DTH = ((2.0*PI)*(L-1))/BN
      THEDH = DDTH/10.0
      THE = 0.0
      THED = 0.0
```

```
      DO 21 LL=1,11
      THED = THE+DTH
      CALL FREE(DGAM1,DGAM2,XR(N),XR(N-1),THE,THED,XMK,TANPHI,VFALL,
     1VFTLL)
      SUMAH = SUMAH+0.5*(VFALL-VFAHL)*(THE-THEO)+(VFAHL)*(THE-THEO)
      SUMTH = SUMTH+0,5*(VFTLL-VFTHL)*(THE-THEO)+(VFTHL)*(THE-THEO)
      VFAHL = VFALL
      VFTHL = VFTLL
      THEO = THE
   21 THE = THEO+THEDH
      DDTH = DDTH+((CHMK*COS(PHIMK))/(4.0*XMK))
      THEDQ = DDTH/20.0
      THE = 0.0
      THEO = 0.0
      DO 22 LL=1,21
      THED = THE+DTH
      CALL FREE(DGAM1,DGAM2,XR(N),XR(N-1),THE,THED,XMK,TANPHI,VFALL,
     1VFTLL)
      SUMAQ = SUMAQ+0.5*(VFALL-VFAQL)*(THE-THEO)+(VFAQL)*(THE-THEO)
      SUMTQ = SUMTQ+0.5*(VFTLL-VFTQL)*(THE-THEO)+(VFTQL)*(THE-THEO)
      VFAQL = VFALL
      VFTQL = VFTLL
      THEO = THE
   22 THE = THEO+THEDQ
      VFAH = VFAH+SUMAH
      VFTH = VFTH+SUMTH
      VFAQ = VFAQ+SUMAQ
      VFTQ = VFTQ+SUMTQ
   20 CONTINUE
      WRITE(3,113)  N,VFAH,VFTH,VFAQ,VFTQ
   13 CONTINUE
      UAKQ = VBAQ+VFAQ-VHAQ
      UAKH = VBAH+VFAH-VHAH
      UTKH = VBTH+VFTH
      UTKQ = VBTQ+VFTQ
      WRITE(3,115) K,UAKH,UTKH,UAKQ,UTKQ
      UKH = SQRT(UAKH*UAKH+UTKH*UTKH)
      UKQ = SQRT(UAKQ*UAKQ+UTKQ*UTKQ)
      GMH = (ATAN(UTKH/(-UAKH)))*(57.29578)
      GMQ = (ATAN(UTKQ/(-UAKQ)))*(57.29578)
      WTK = (WT(K)+WT(K-1))/2.0
      WAK = (WA(K)+WA(K-1))/2.0
      W = SQRT(WAK**2.0+WTK**2.0)
      GMW = (ATAN(WTK/WAK))*(57.29578)
      WRITE(3,116) UKH,UKQ,GMH,WTK,WAK,W,GMW
      VEH = (VE(K)+VE(K-1))/2.0
      DUKH = (UKH-W)/VEH
      DUKQ = (UKQ-W)/VEK
      ALPHK = DUKH
      ALPHD  = ALPHK*57.29578
      SLOPE = ALPHK-DUKQ
      CLILS  =(-11.4385)*SLOPE
      ZMKLS = (-0.6309)*SLOPE
```

```
      ZMLSC = (-0.5)*SLOPE
      VCK = (VC(K)+VC(K-1))/2.0
      ALAM = ATAN(((VCK+WAK)*(WTK)*2.0)/((PI*XMK/AJ)*((PI*XMK/AJ)-
     1  (2.0*WTK))+(VCK+WAK)**2.0
      DELZM = (1.0-COS(ALAM/2.0))/ALAM
      CLIK = (CLI(K)+CLI(K-1))/2.0
      ZMKLL = (0.5516*CLIK) +DELZM
      WRITE(3,117) ALPHD,CLILS,CLIK,ZMKLS,ZMLSC,DELZM,ZMKLL
   12 CONTINUE
   15 CONTINUE
      CALL EXIT
      END
```

A description of variables of Subroutine VELO will be found in Appendix H of Reference 10.

Description of the FORTRAN Program

This program applies the methods developed in Chapters II and V for solving for the blade section characteristics. The program first reads in an 80-character title, the number of cases being considered. It next reads the starting section of the blade, the number of blades, the advance ratio and the axial coordinate of the 1/4 chord point. Just as in the propeller interference program, this program next reads in the card output of the lifting line design program. Once all the data has been read in, it is printed out by the computer.

Subroutine VELO is then called which reads in the coordinates of the body and hub ring sources, as well as their strengths after control is returned to the main program, and a loop is entered that considers the control points of each of the blade sections. Once the values of velocity to be calculated have been initialized, the main program determines the axial coordinates of both the 1/2 chord and the 3/4 chord points. Entry point CAVEL of subroutine VELO is then called twice for each of these points. Details of this program can be found in Appendix G of Reference 10. This subroutine returns to the main program with the values of axial induced velocities at the 1/2 and 3/4 chord points due to the source distribution over the body. The main program next enters a loop where it considers the elements of vorticity along the blade. Mean values of chord, pitch angle and radial distance are than calculated as well as values of θ. Subroutine BOUN is then called twice to find the values of velocity induced by that particular segment of the bound vorticity. This subroutine represents Equation (25) and (26) of Chapter II. By means of a loop, the effect of all the blades is summed. The program next calculates the strength of the free vortex around the segment of bound

vortex under consideration. Next, values used in the numerical integration of the free vortex effects are initialized. The length of free vorticity from the 1/4 chord point to the 1/2 chord point is broken up into 10 divisions for the integration. A loop is then entered that numerically integrates this effect to the 1/2 chord point. In this loop, subroutine FREE is called which represents Equation (40) and (41) of Chapter II. Likewise, the free vortex effect at the 3/4 chord point is calculated by numerically integrating over the larger distance that is broken up into 20 segments. As before, the effects of the other blades are also considered. This procedure is repeated for all segments of vorticity along the blade.

Once these velocities are summed over the entire blade vortex system, their components are added with the output of entry point CAVEL and printed out. The magnitudes and the angles of the velocities are then found. Next, the induced velocity from the lifting line program is used with the velocities above to calculate Equations (63) and (64) of Chapter V. Equations (66) and (68) are subsequently used to solve for the ideal lift coefficient of the lifting surface and the maximum camber. Maximum camber of the circular arc airfoil is then found via Equation (70) of Chapter V. The maximum camber of the lifting line solution is then solved for and all the results are printed out. This entire process is repeated for each section of the blade. Approximate running time for 21 sections on the IBM 370/168 is 60 seconds.

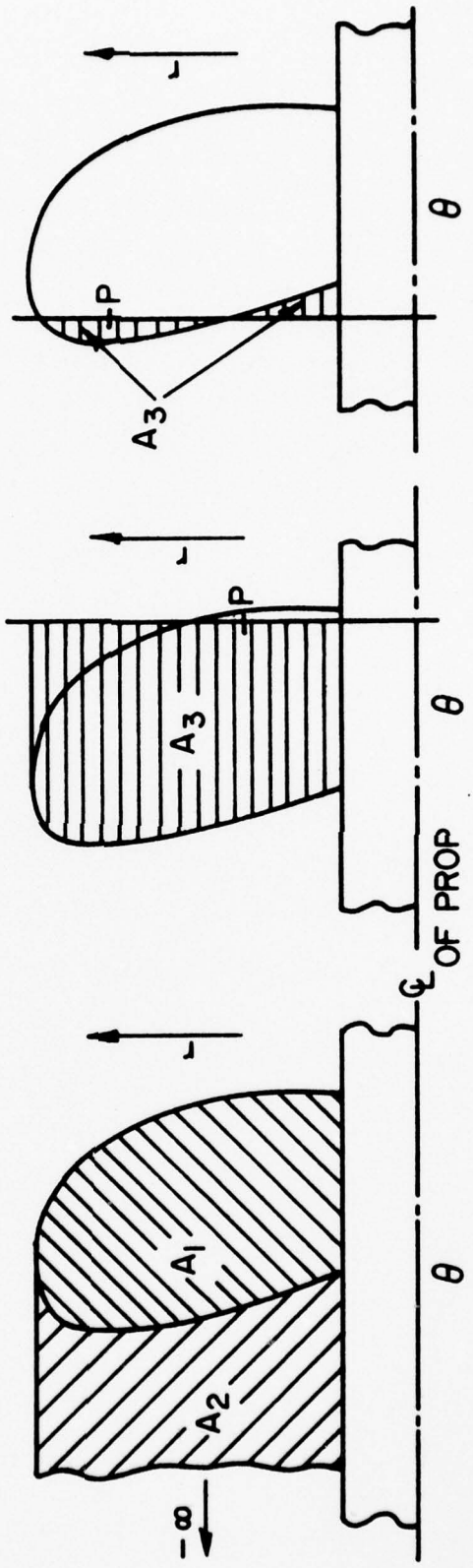

Figure 1: Various Areas of Integration

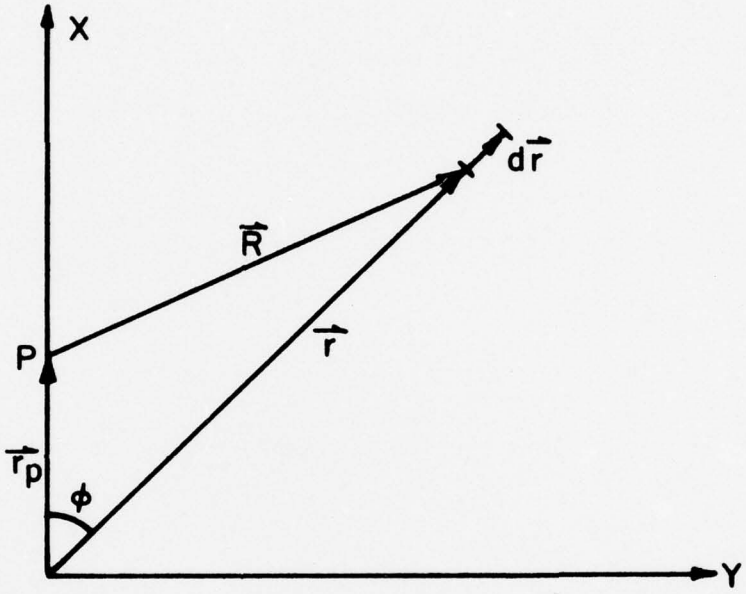

Figure 2: Geometry of Bound Vortex System

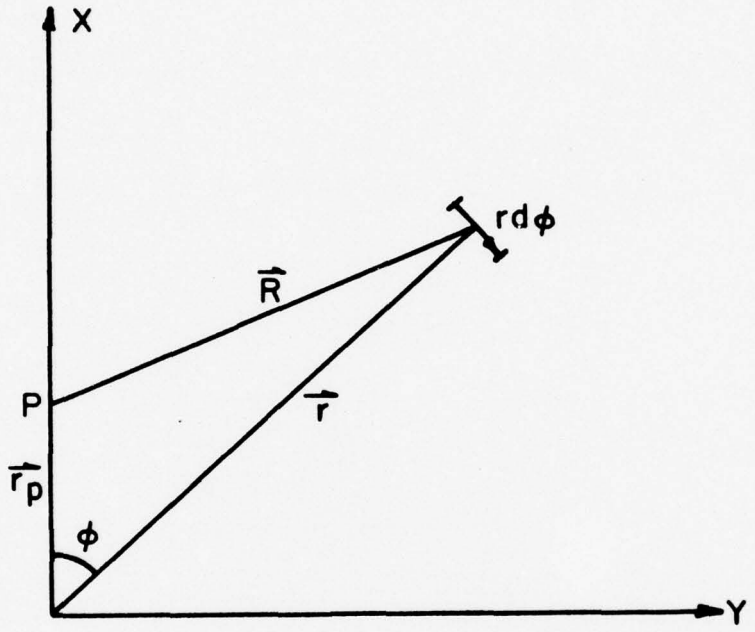

Figure 3: Geometry of Free Vortex System

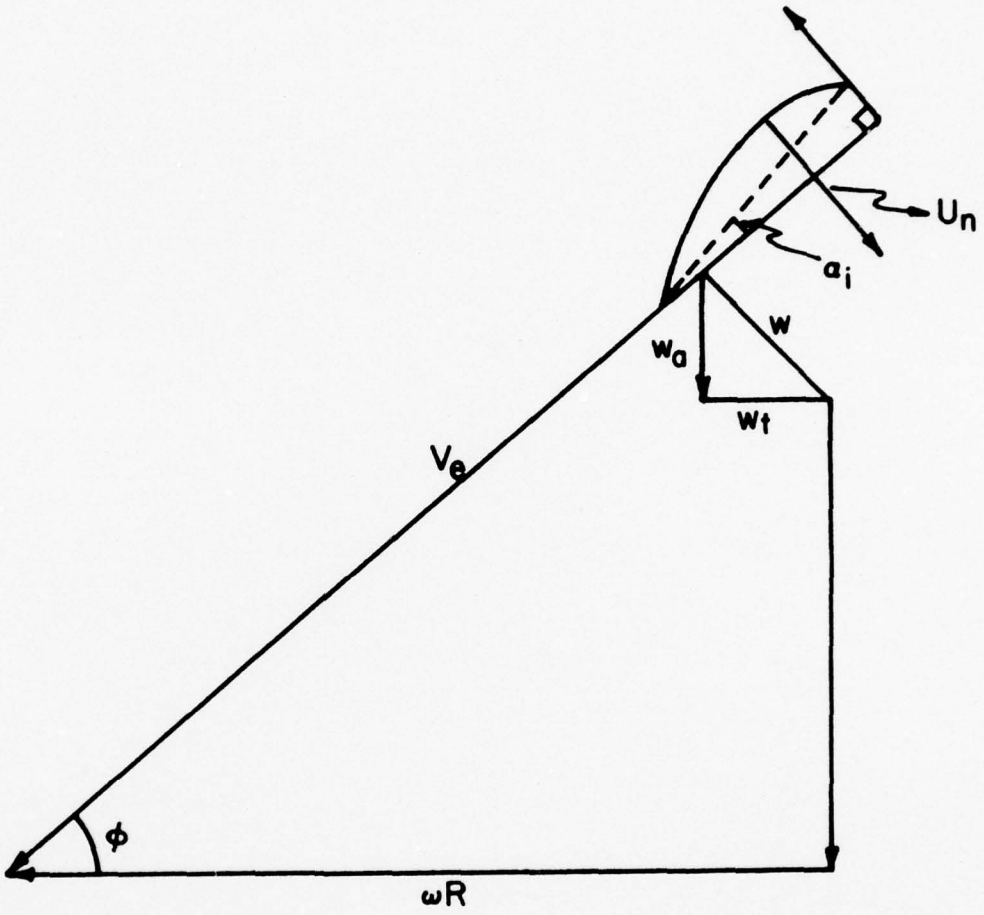

Figure 4: Propeller Velocity Diagram

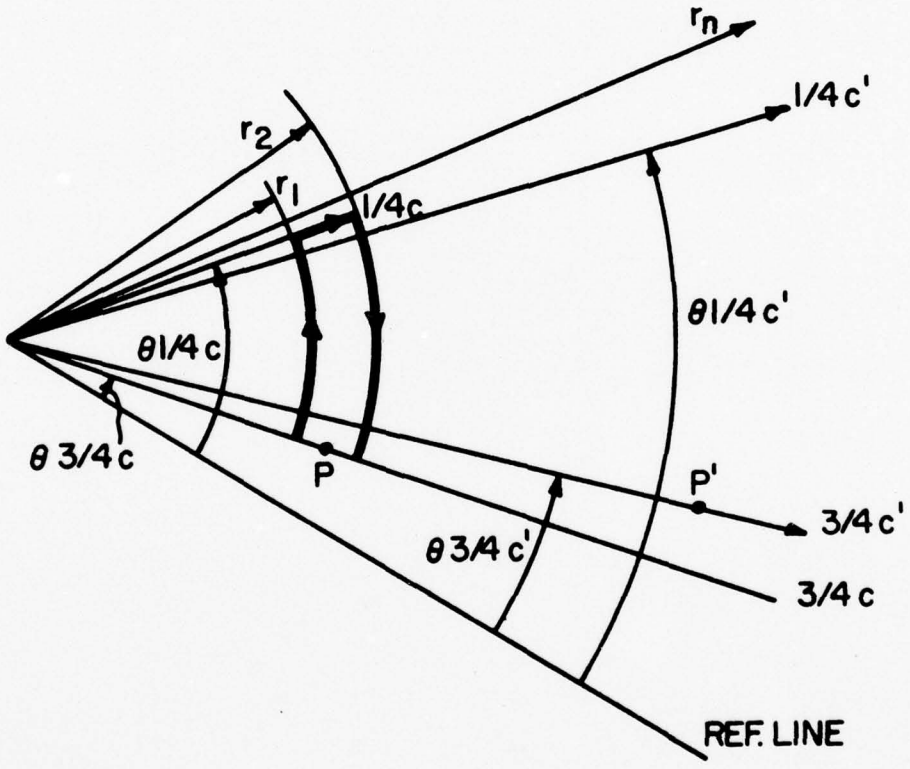

Figure 5: Diagram of Limits of Integration

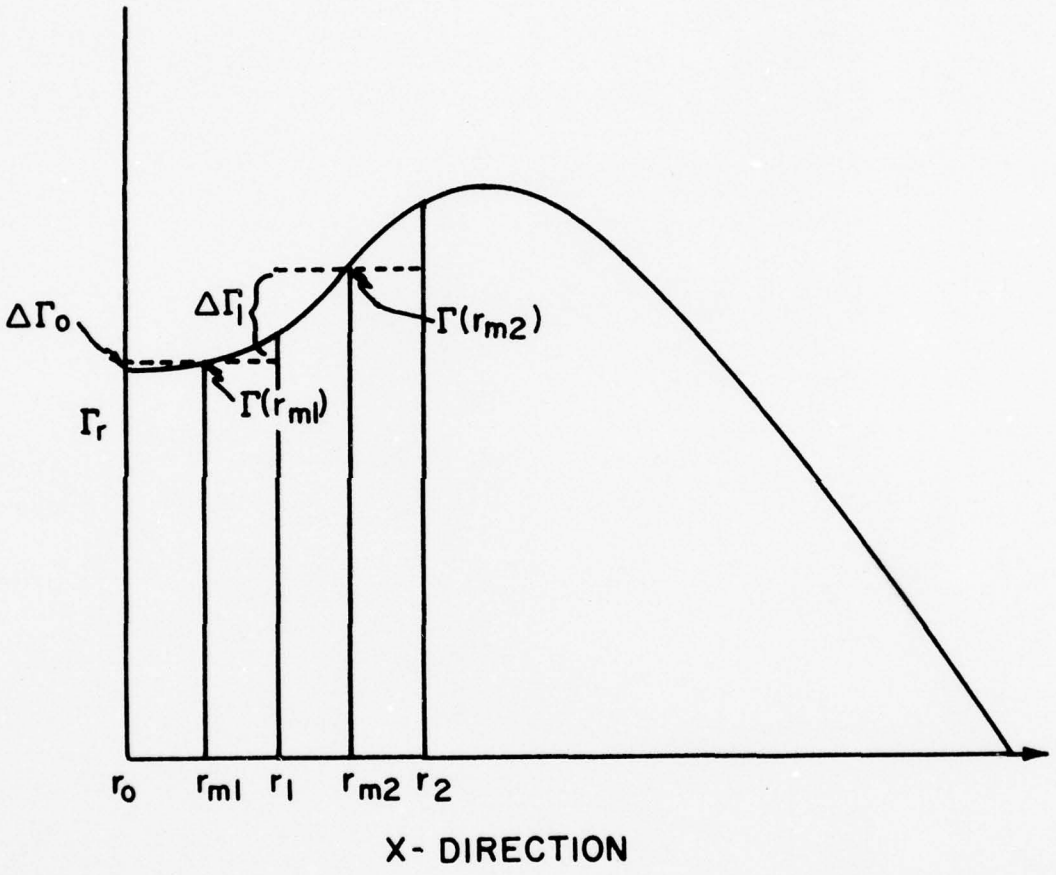

Figure 6: Circulation Distribution

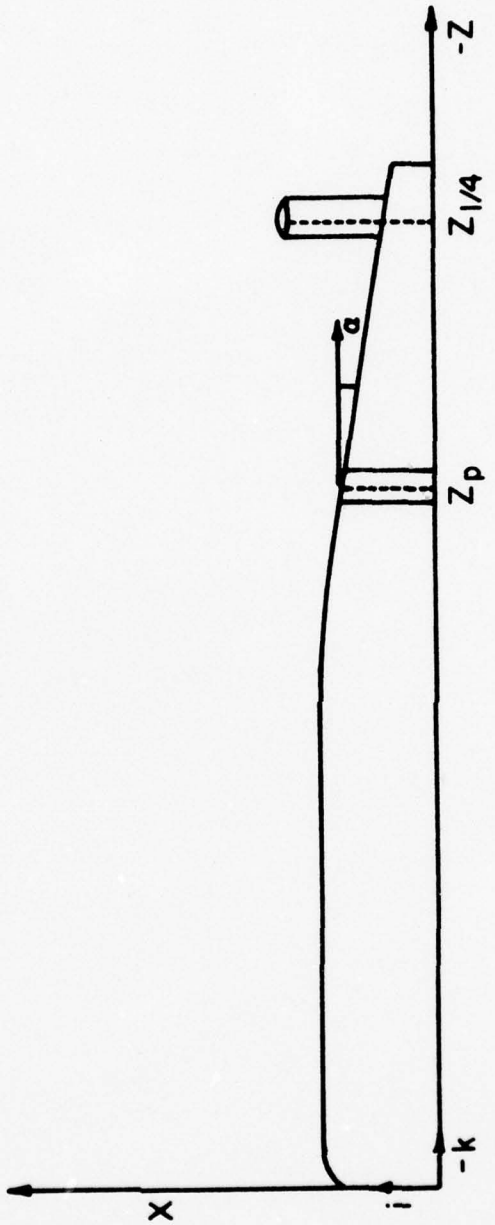

Figure 7: Submerged Body

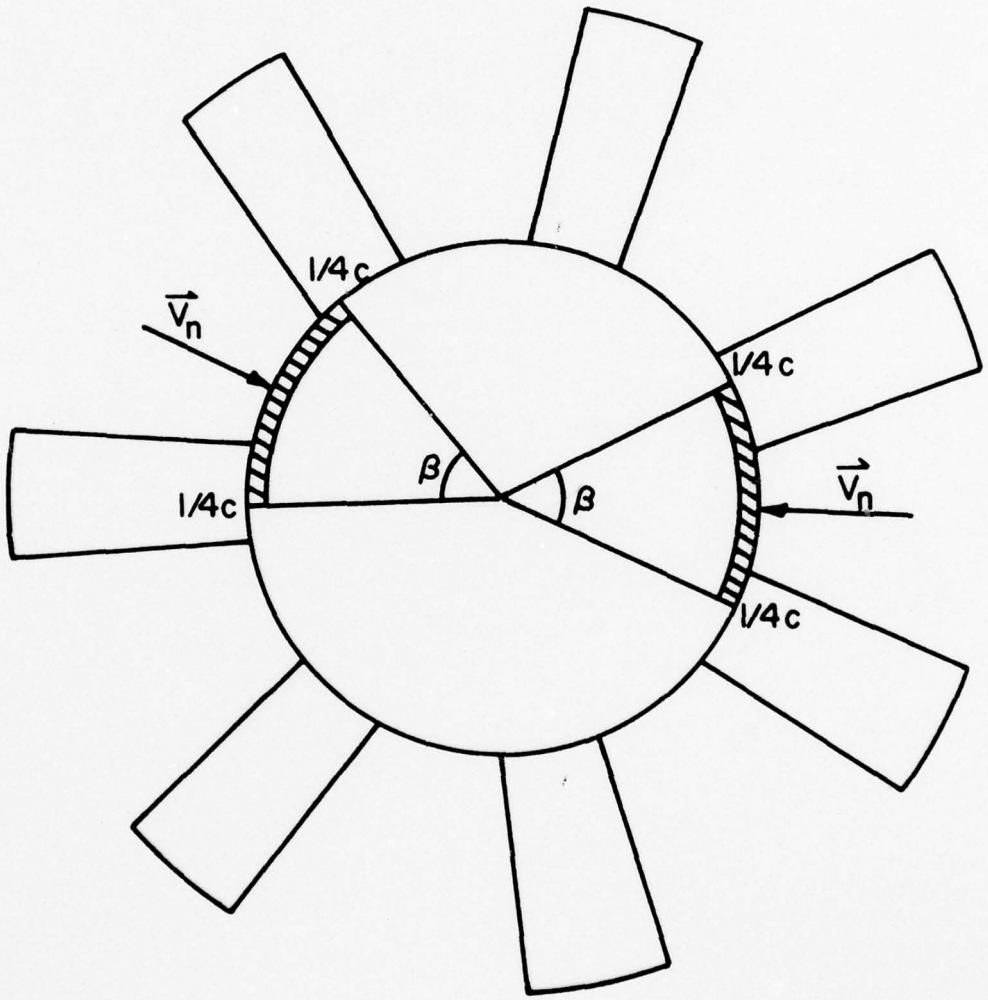

Figure 8: Average Induced Velocity Normal to the Hub

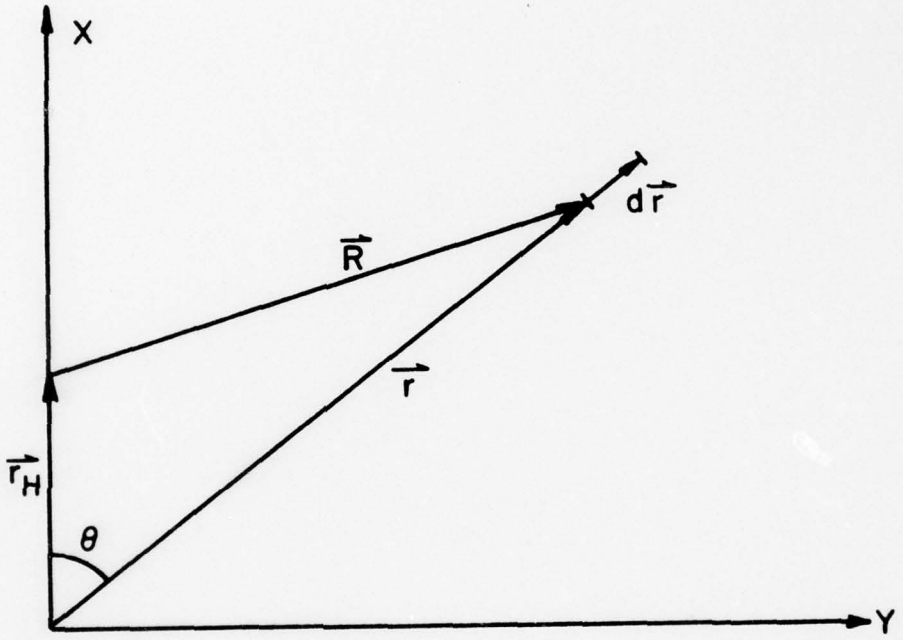

Figure 9: Geometry of Bound Vortex System at the Hub

AD-A047 565 PENNSYLVANIA STATE UNIV UNIVERSITY PARK APPLIED RESE--ETC F/G 13/10
PROPELLER-HUB INTERFERENCE EFFECTS USING AN APPROXIMATE LIFTING--ETC(U)
JUN 77 K LUDOLPH N00017-43-C-1418
UNCLASSIFIED TM-77-198 NL

2 OF 2
AD
A047 565

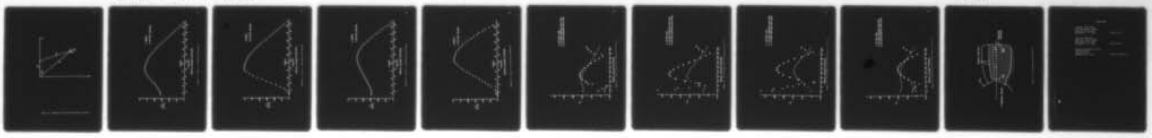

END
DATE FILMED
1-78
DDC

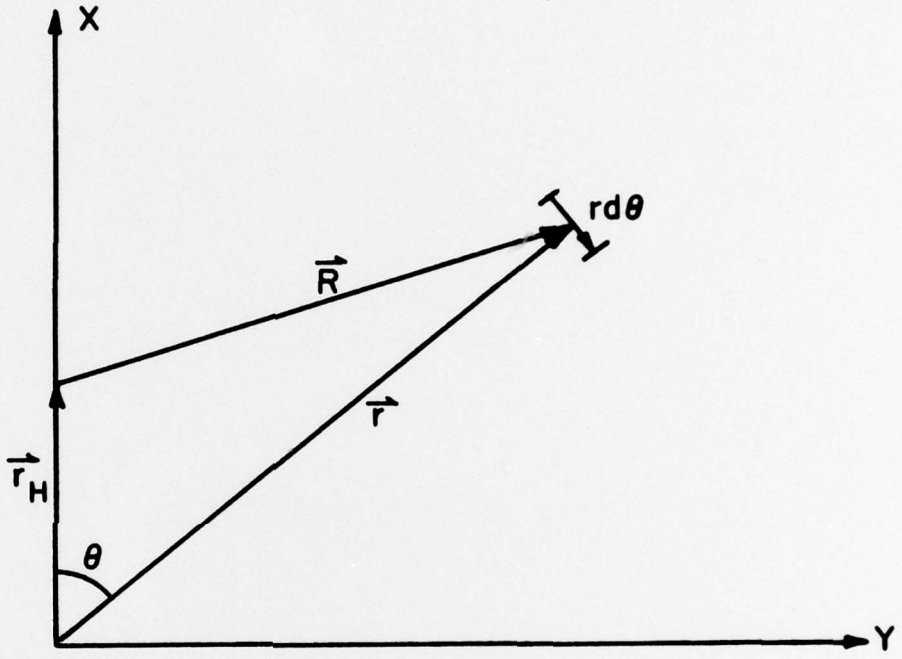

Figure 10: Geometry of Free Vortex System at the Hub

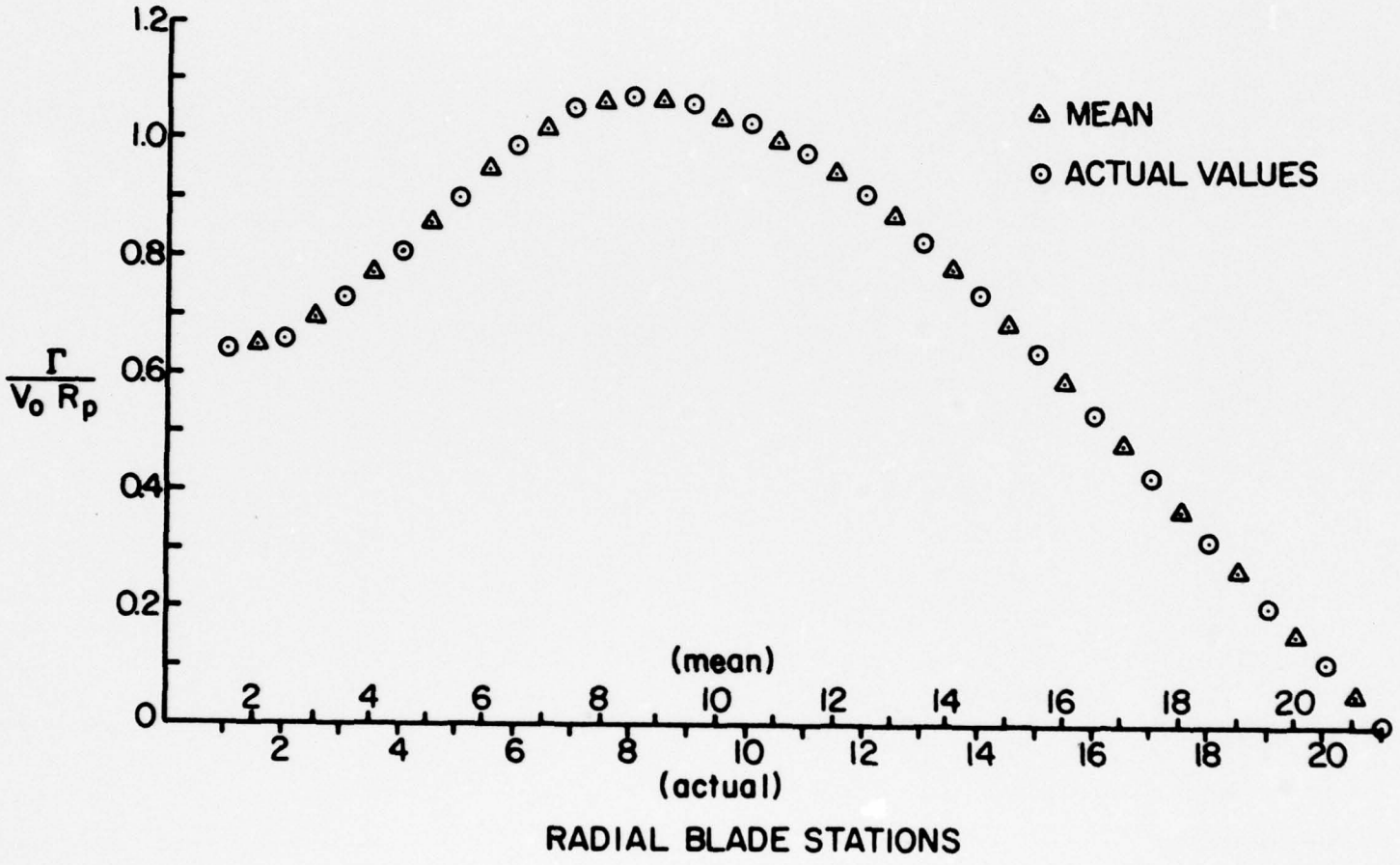

Figure 11: Case I: Circulation Distribution

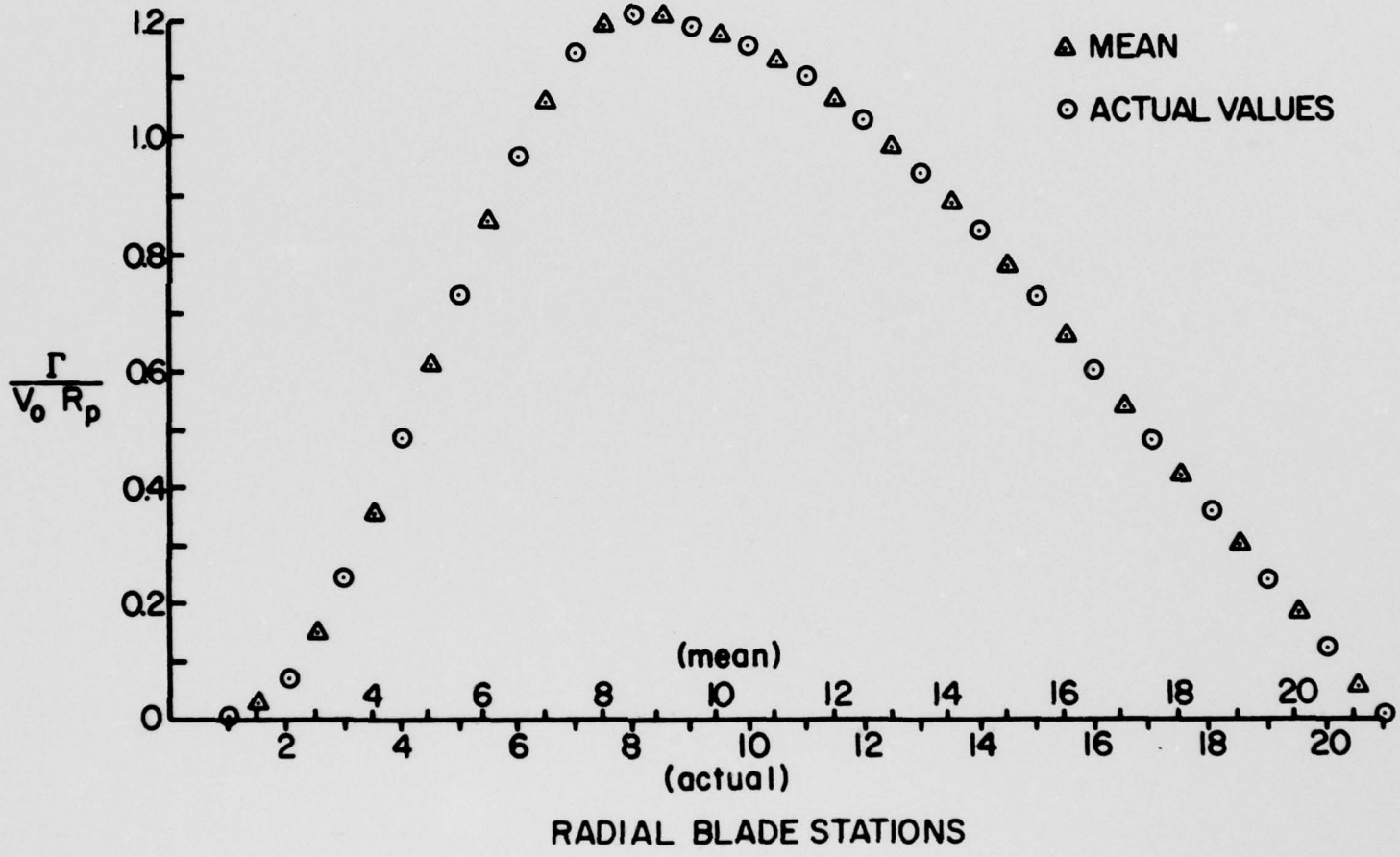

Figure 12: Case II: Circulation Distribution

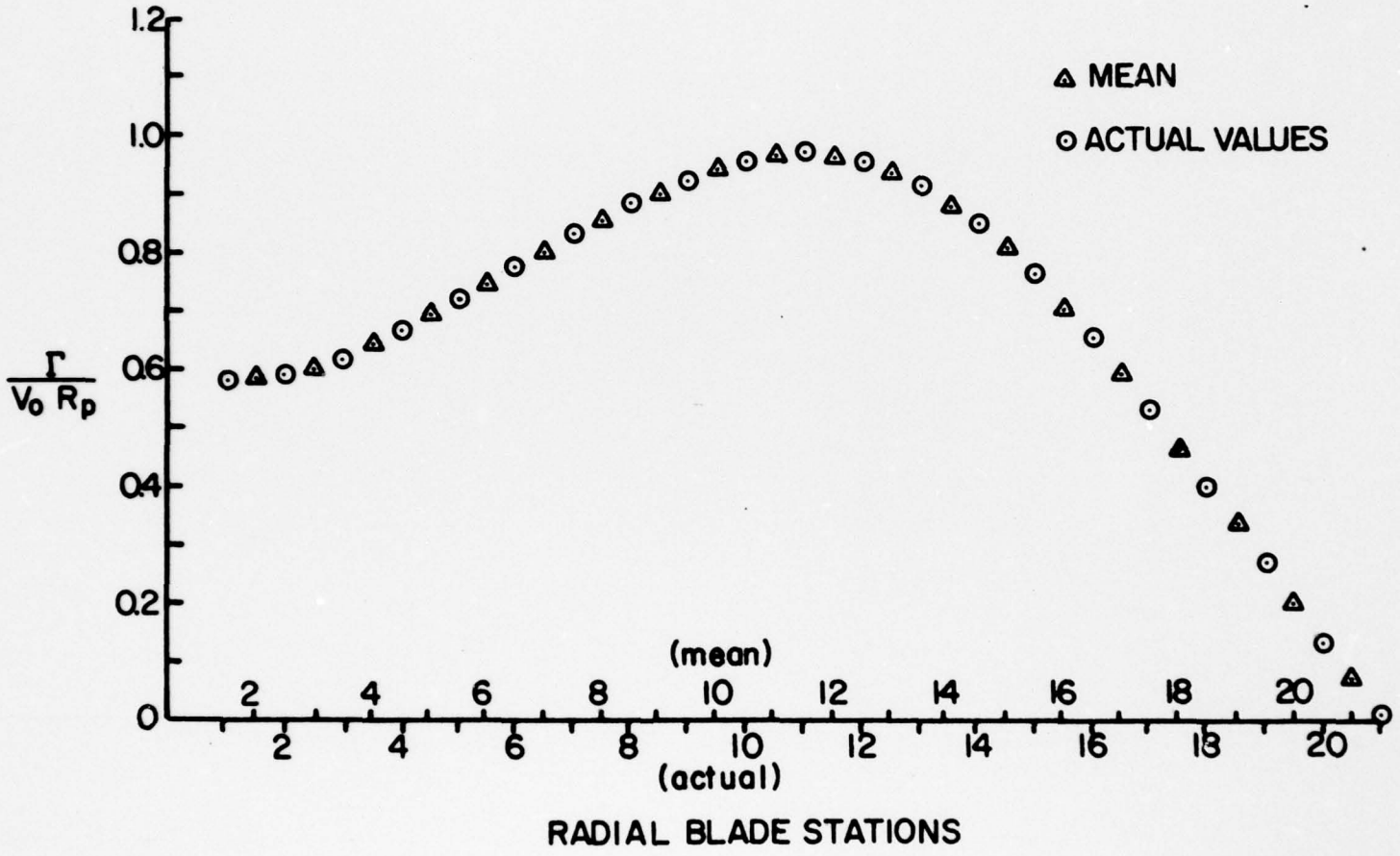

Figure 13: Case III: Circulation Distribution

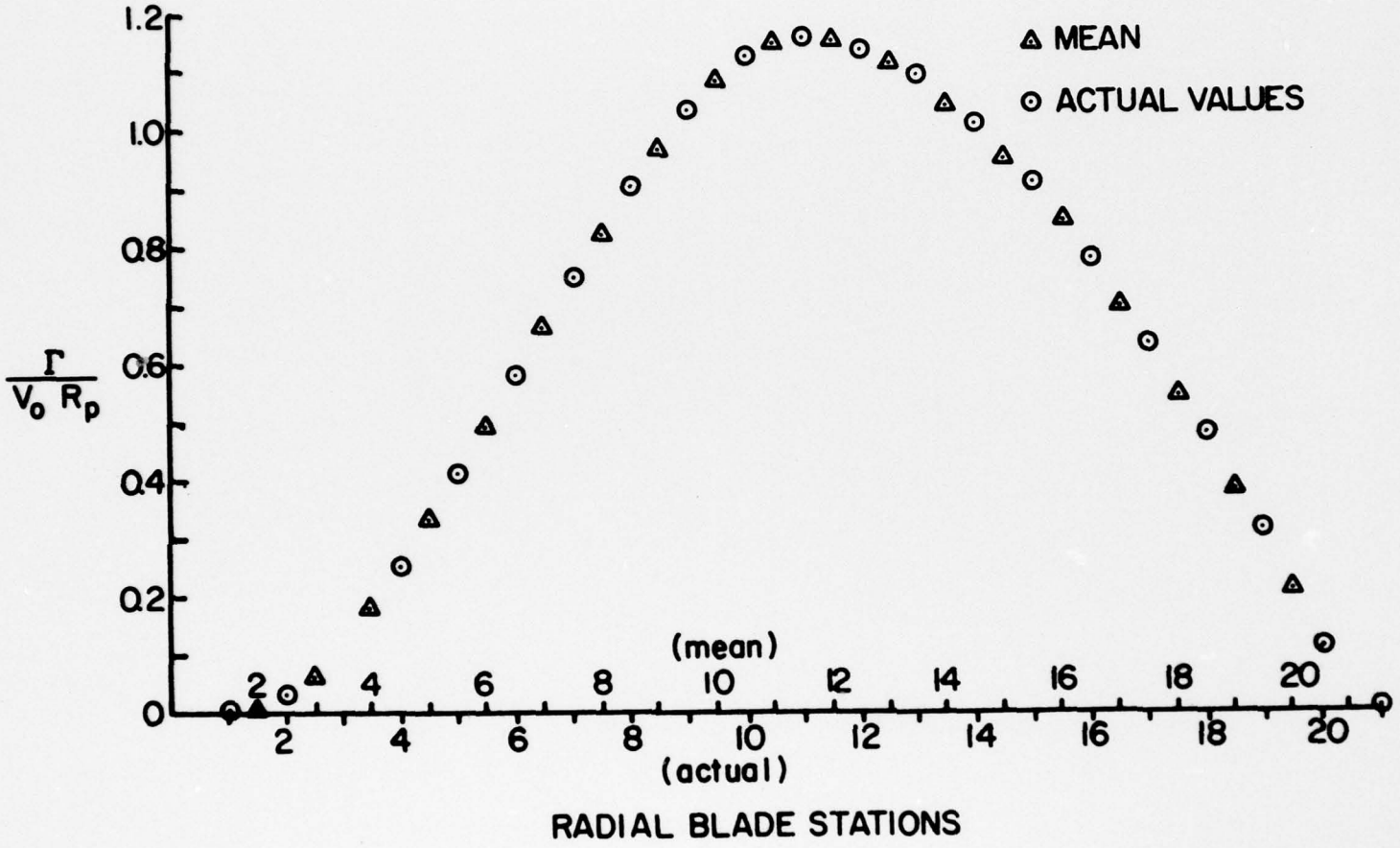

Figure 14: Case IV: Circulation Distribution

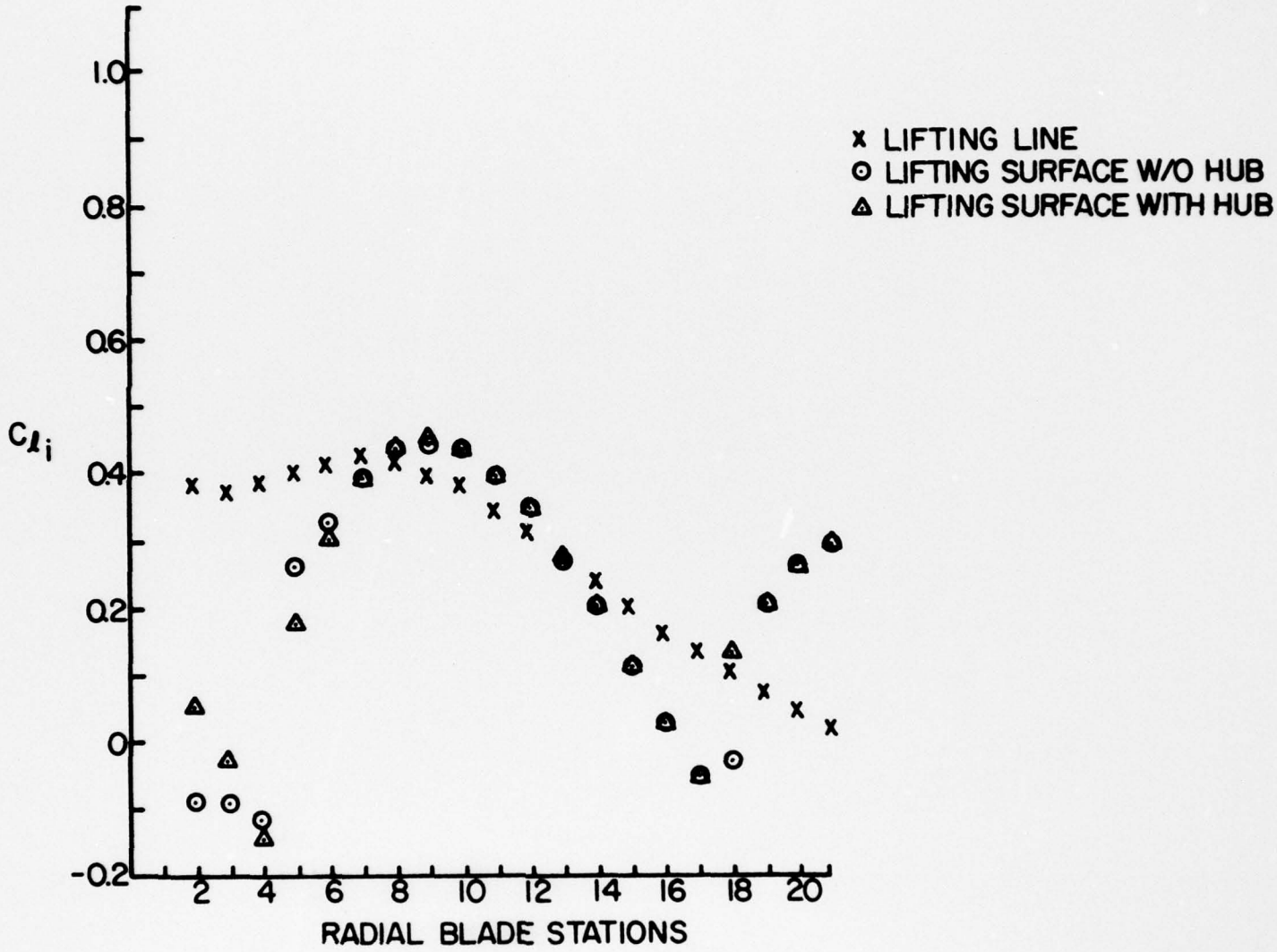

Figure 15: Plot of Ideal Lift Coefficients for Case I

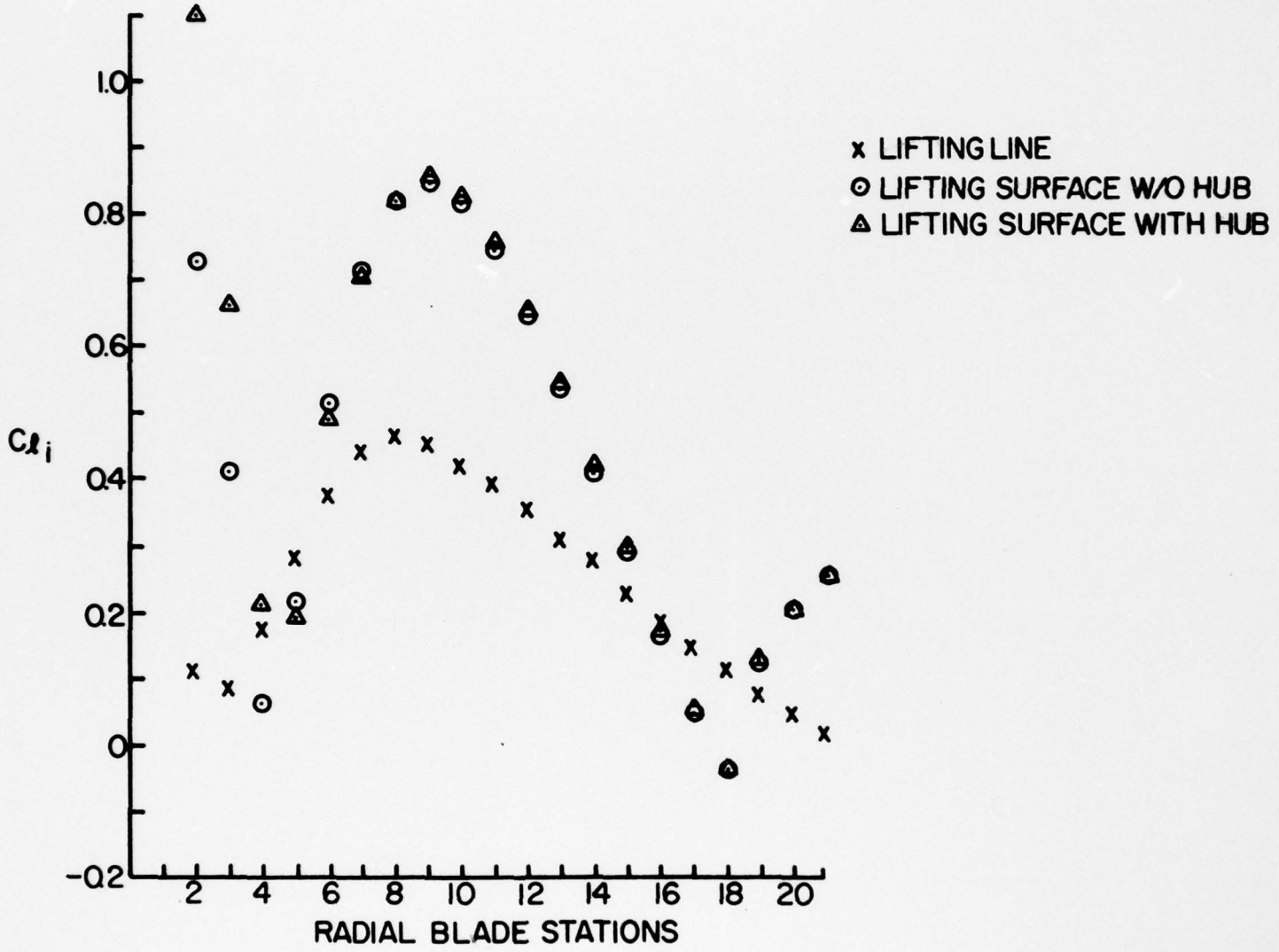

Figure 16: Plot of Ideal Lift Coefficients for Case II

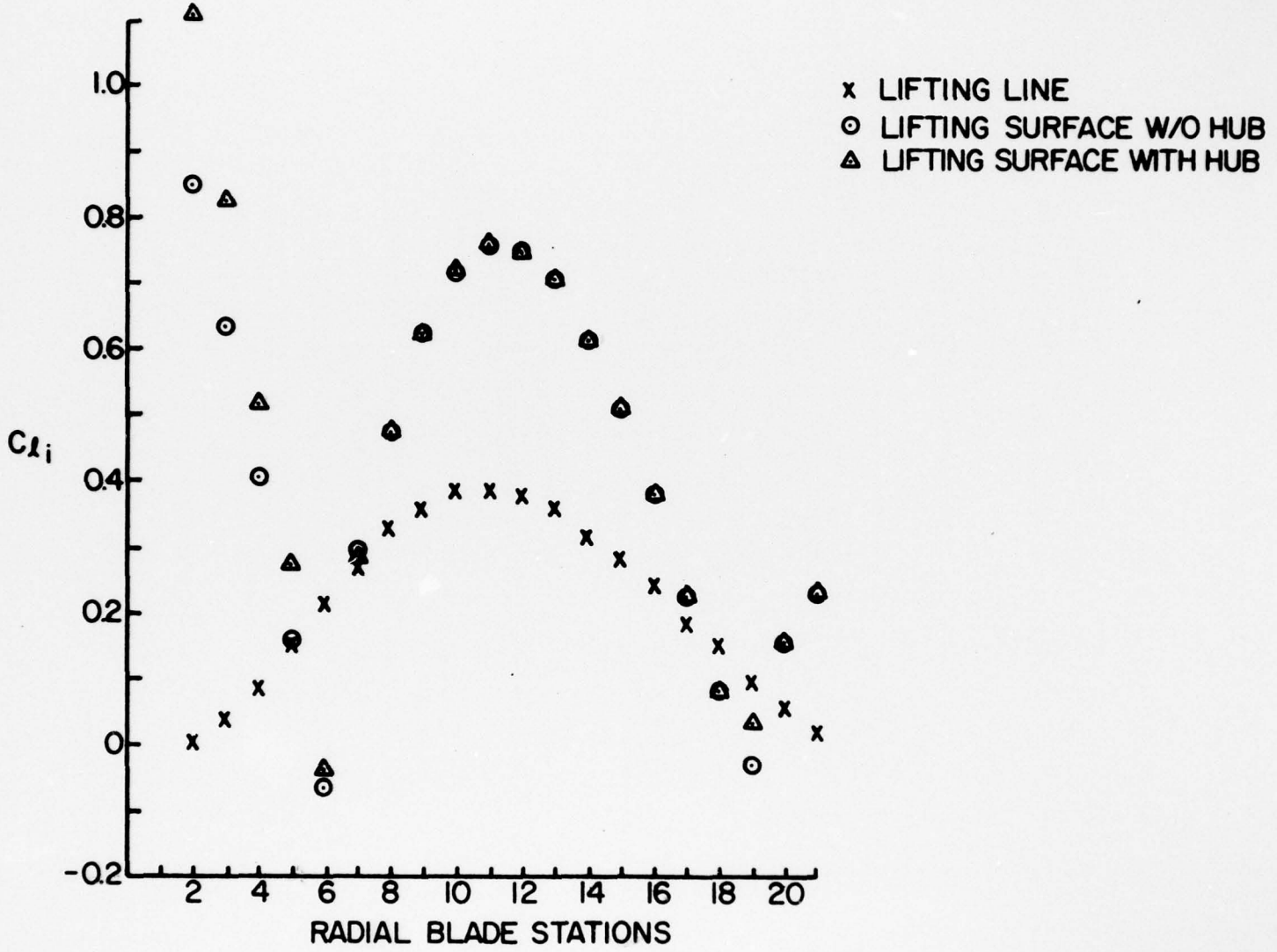

Figure 17: Plot of Ideal Lift Coefficients for Case III

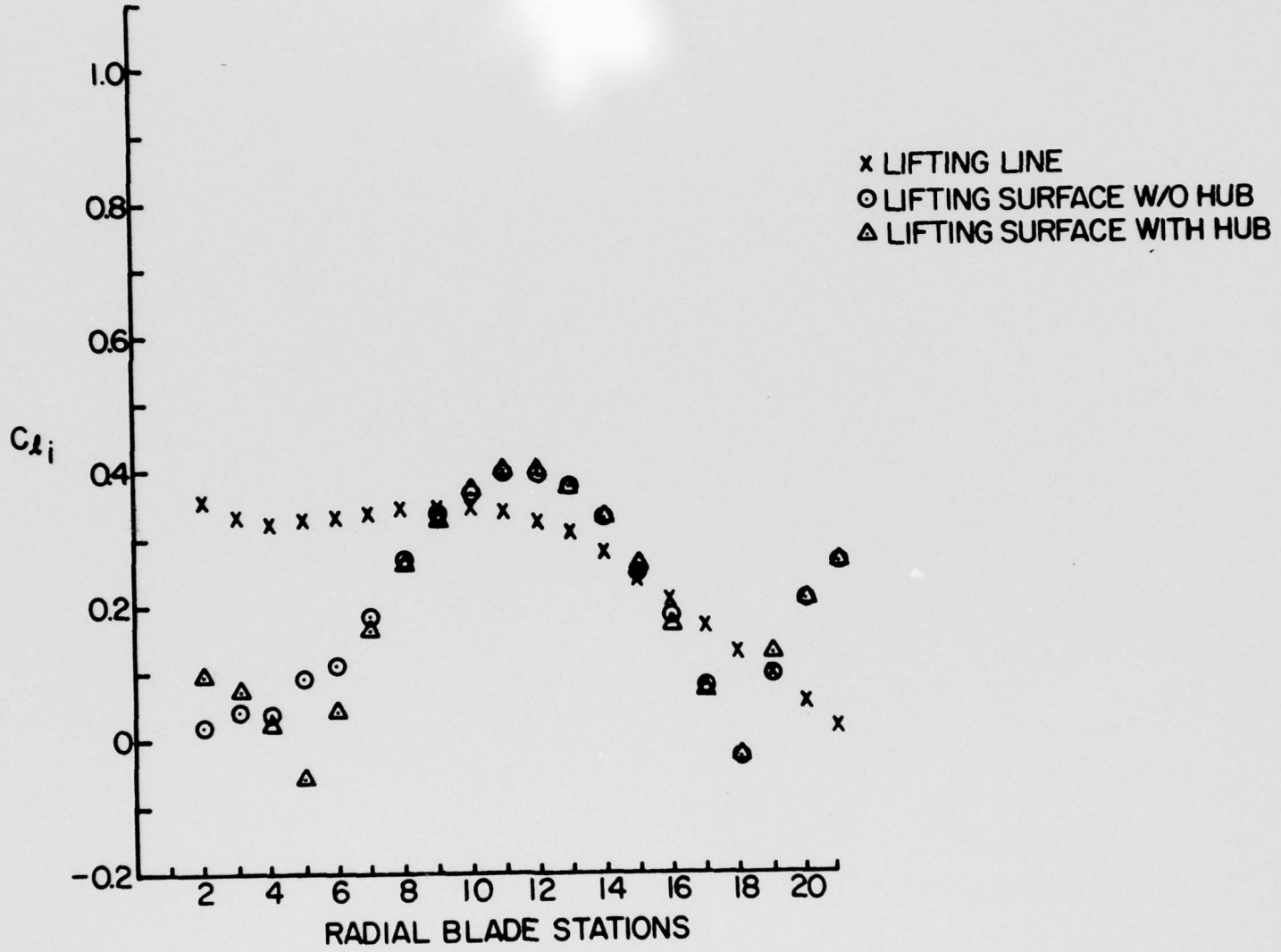

Figure 18: Plot of Ideal Lift Coefficients for Case IV

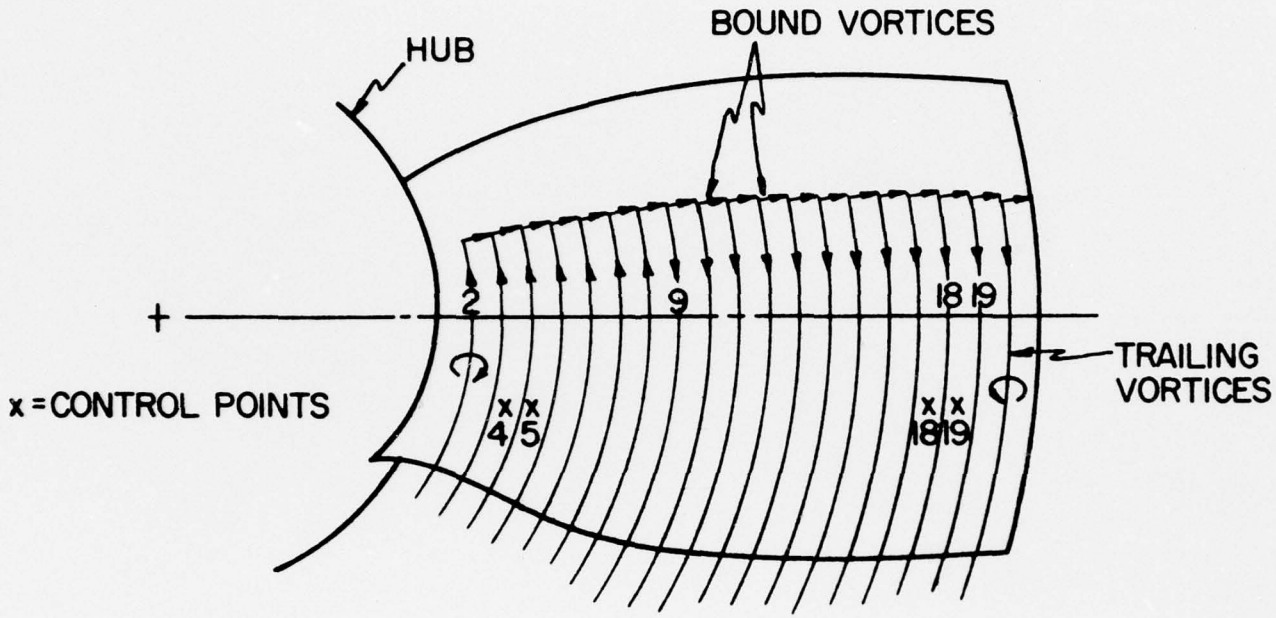

Figure 19: The Blade Free Vortex System

DISTRIBUTION

Commander (NSEA 09G32)
Naval Sea Systems Command
Department of the Navy
Washington, D. C. 20362 — Copies 1 and 2

Commander (NSEA 0342)
Naval Sea Systems Command
Department of the Navy
Washington, D. C. 20362 — Copies 3 and 4

Defense Documentation Center
5010 Duke Street
Cameron Station
Alexandria, VA 22314 — Copies 5 through 16